Missouri State University

BearWorks

MSU Graduate Theses

Summer 2022

Analysis of Root System Architecture and QTL Identification in Grapevines

Sujan Thapa
Missouri State University, st25s@MissouriState.edu

As with any intellectual project, the content and views expressed in this thesis may be considered objectionable by some readers. However, this student-scholar's work has been judged to have academic value by the student's thesis committee members trained in the discipline. The content and views expressed in this thesis are those of the student-scholar and are not endorsed by Missouri State University, its Graduate College, or its employees.

Follow this and additional works at: https://bearworks.missouristate.edu/theses

 Part of the Botany Commons, Cell and Developmental Biology Commons, Genetics Commons, Molecular Genetics Commons, Plant Biology Commons, and the Viticulture and Oenology Commons

Recommended Citation

Thapa, Sujan, "Analysis of Root System Architecture and QTL Identification in Grapevines" (2022). *MSU Graduate Theses*. 3778.
https://bearworks.missouristate.edu/theses/3778

This article or document was made available through BearWorks, the institutional repository of Missouri State University. The work contained in it may be protected by copyright and require permission of the copyright holder for reuse or redistribution.
For more information, please contact BearWorks@library.missouristate.edu.

ANALYSIS OF ROOT SYSTEM ARCHITECTURE AND QTL IDENTIFICATION IN GRAPEVINES

A Master's Thesis

Presented to

The Graduate College of

Missouri State University

In Partial Fulfillment

Of the Requirements for the Degree

Master of Science, Biology

By

Sujan Thapa

August 2022

© 2022, Sujan Thapa

ANALYSIS OF ROOT SYSTEM ARCHITECTURE AND QTL IDENTIFICATION IN GRAPEVINE

Biology

Missouri State University, August 2022

Master of Science

Sujan Thapa

ABSTRACT

The root system of the plant plays a vital role in water and nutrient uptake. Native North American grapevines adapted to a broad range of climatic and soil conditions, which led to the evolution of diverse root system architecture (RSA) within the *Vitis* genus. Despite the importance of RSA in viticulture, little is known about the genetic basis of the RSA in grapevine. I used novel root phenotyping tool, RhizoVision Analyzer to characterize the root system of 208 genotypes of an F_1 grapevine progeny obtained from a cross between *Vitis rupestris* Scheele B38 and *Vitis riparia* Michx. HP-1. Dormant cuttings from these genotypes were grown for five weeks in controlled atmospheric conditions, and then twenty-six RSA traits were extracted from 2-D root images. Forty-seven female parental cuttings were also rooted, which enabled calculation of environmental and genetic variance in the F_1 population. High heritability was found for number of root tips, total root length, and holes. Principal component analysis (PCA) conducted with diverse traits, demonstrated that PC1 explained 40.03% variation and it correlated well with medium angle frequency. A negative correlation was found between average root diameter and the number of root tips and total root length of the root system. Total root length, number of root tips, maximum and median number of roots were found to be significantly different between the female parent and the F_1 population. Quantitative trait locus (QTL) analysis was conducted and genetic regions influencing total root length, maximum width, and surface area were identified in chromosome 2. Calcium, magnesium and zinc were found to be positively correlated with traits that increase the size of the root system. Canonical correspondence analysis (CCA) showed that manganese was associated with coarse diameter frequency and number of root tips, whereas iron was associated with medium angle frequency. The findings presented here offer insights into the genetic makeup of RSA in grapevine and provide breeders with actionable information to develop grapevine varieties that are better adapted to conditions brought by climate change.

KEYWORDS: root system architecture, 2-D imaging *Vitis rupestris, Vitis riparia,* QTL, linkage mapping, F_1 hybrids

ANALYSIS OF ROOT SYSTEM ARCHITECTURE AND QTL IDENTIFICATION IN GRAPEVINE

By

Sujan Thapa

A Master's Thesis
Submitted to the Graduate College
Of Missouri State University
In Partial Fulfillment of the Requirements
For the Degree of Master of Science, Biology

August 2022

Approved:

Laszlo G. Kovacs, Ph.D, Thesis Committee Chair

Debra S. Finn, Ph.D, Committee Member

Michelle Bowe, Ph.D, Committee Member

Julie Masterson, Ph.D, Dean of the Graduate College

In the interest of academic freedom and the principle of free speech, approval of this thesis indicates the format is acceptable and meets the academic criteria for the discipline as determined by the faculty that constitute the thesis committee. The content and views expressed in this thesis are those of the student-scholar and are not endorsed by Missouri State University, its Graduate college, or its employees.

ACKNOWLEDGEMENTS

I would like to thank my major advisor Dr. Laszlo G. Kovacs for providing support and guidance throughout my study, course work, and research activities. I am especially thankful for his guidance, patience, and his availability to always answer questions. I am also grateful to my thesis committee members Dr. Debra S. Finn, and Dr. Michelle Bowe for the guidance they provided to my thesis research. I am also very thankful for the support provided by the Graduate College and the Department of Biology at Missouri State University and the National Science Foundation Plant Genome Research Program (NSF-PGRP) which made this research project possible. I want to express my heartful gratitude to Dr. Courtney Coleman, Hunter Bartelt, and Eli Ascencio for their help and support for various aspects of my research. I would also like to thank all my teachers at Missouri State University.

I dedicate this thesis to my family.

TABLE OF CONTENTS

Introduction 1
Methodology 6
Plant Materials and Preparation 6
Root System Photographing and Data Extraction 7
Mapping Population, Genotyping, and QTL Mapping 8
Analysis 9
Results 12
Root Trait Heritability and Contrasts Between F1 Progeny and Their Female Parent 12
Correlation Between Various Root Traits and Leaf Elemental Concentrations 12
Principal Component and Canonical Correspondence Analyses 13
QTL for Root Traits 14
Discussion 16
References 23
Appendices 43
Appendix A. Script used in R/qtl for QTL peak detection 43
Appendix B. Data used to create diagram for maximum width QTL in MapChart 44
Appendix C. Data used to create diagram for surface area QTL in MapChart 45
Appendix D. Data used to create diagram for total root length QTL in MapChart 46
Appendix E. Correlation values between root traits and leaf elemental concentration through various growth stages 48

ABBREVIATIONS

A	Arsenic
ahs	Average hole size
aro	Average root orientation
B	Boron
CCA	Canonical correspondence analysis
Cd	Cadmium
cdr	Coarse diameter frequency
Chr	Chromosome
CV%	Coefficient of variation
Fe	Iron
K	Potassium
maf	Medium angle frequency
Max	Maximum
Min	Minimum
Mn	Manganese
Mo	Molybdenum
MS	Microsoft
N	North
Na	Sodium
P	Phosphorus
PCA	Principal component analysis
QTL	Quantitative trait loci
RSA	Root system architecture
rt	Number of root tips
S	Sulphur
saf	Shallow angle frequency
SD	Standard of deviation
USDA-ARS	United States Department of Agriculture-Agriculture Research Service
Var	Variation
V_E	Environmental variance
V_G	Genetic variance
V_P	Phenotypic variance
W	West
wdr	width-to-depth ratio

LIST OF TABLES

Table 1. Twenty-six RSA traits extracted from 2-D images of root system..... 28

Table 2.Traits measured in the female parent and the F1 progeny.. 29

LIST OF FIGURES

Figure 1. Diagrammatic representation of the experimental setup to root dormant cuttings. 30

Figure 2. Example of F1 genotypes excluded as outliers from analysis. 30

Figure 3. Range of RSA traits of F1 progeny and their female parent. 31

Figure 4. Pearson correlation matrix of RSA traits. 32

Figure 5. Pearson correlation matrix of RSA traits and leaf elemental concentration 33

Figure 6. PCA analysis of seven diverse RSA traits 34

Figure 7. CCA biplot of the relationship between RSA traits and leaf elemental concentration . 35

Figure 8. QTL mapping of the maximum width of the root system 36

Figure 9. QTL mapping of the surface area of the root system. 37

Figure 10. QTL mapping of the total length of the root system. 38

Figure 11. QTL for the width-to-depth ratio 39

Figure 12. QTL for the network area 39

Figure 13. QTL for the lower root area 40

Figure 14. QTL for the maximum diameter 40

Figure 15. Correlation between average diameter and total root length 41

Figure 16. Correlation between average diameter and root size determining traits 42

INTRODUCTION

Climate change poses a serious threat to global food production (Smith 2010; Liu et al. 2013; Jia et al. 2019). Climate change is causing a shift on crop growing seasons and its impact will likely be more prominent in the coming decades (Gomez-Zavaglia et al. 2020). The rise in global temperature has led to erratic rainfall and more frequent droughts, floods, heatwaves, and extreme weather events throughout the globe (Arora 2019). Irregular heavy rainfall and flashfloods reduce the drainage of rainwater by 17% (Mishra 2017). These flash floods impair groundwater replenishment and create freshwater shortages for irrigation and human consumption (Sen 2021). In addition, consumers are increasingly conscious of purchasing food produced in an environmentally responsible manner. To meet the challenges of both the climate crisis and the demands of consumers, plant breeders must develop new crop varieties that can tolerate extreme environmental conditions and can be cultivated with minimal harm to the environment (Khan et al. 2016).

Grape is one of the most economically important fruit crops grown worldwide and has been cultivated for over 7,000 years (Zhou et al. 2017). After the outbreak of the phylloxera (*Daktulosphaira vitifoliae*) epidemic in Europe, inadvertently introduced from its native range in North America, grafting of the Eurasian grape (*Vitis vinifera*) to American *Vitis* rootstock has become nearly ubiquitous in grapevine-producing regions of the world. Phylloxera is an aphid-like insect which feeds on the roots of all *Vitis*, and causes serious damage in *V. vinifera*, but not in American *Vitis* species (Wilmink et al. 2022). Hence, grafting *V. vinifera* on American rootstock prevents the phylloxera from harming the scion. Of the 70-80 rootstock varieties commonly used today, most were developed in the late 19th century by hybridizing three

American grape species: *Vitis riparia*, *Vitis rupestris*, and *Vitis cinerea* (Ollat et al. 2016). These *Vitis* species are naturally resistant to phylloxera and have also adapted to a diverse variety of biotic and abiotic environmental conditions, such as soil salinity, nematode infestation, or drought (Ollat et al. 2016). Given the widespread use of rootstocks throughout the world, learning about their root development and architecture is even more important. Until recently, grape breeders have focused on the aboveground parts of the vine and paid scarce attention to the features of the root system. Tailoring the architecture of the root system to suit the environment offers a new approach to increasing the sustainability of grape production.

Based on the genetic resources of North American grapevine species, breeders have developed rootstocks to meet a range of challenges in the soil environment. Selecting a proper rootstock that is a good fit for the environment is the most important step in vineyard establishment, as it plays a crucial role in vine health, vigor, and the yield and quality of the fruit throughout the entire lifespan of the vineyard. Rootstocks developed from North American *Vitis* species possess tolerance against phylloxera (Granett et al. 2001), nematodes (Doucleff et al. 2004; McKenry et al. 2004; McKenry and Anwar 2006; Agüero et al. 2013), and salinity (Walker et al. 2004; Hepaksoy et al. 2006). Furthermore, rootstocks also play a prominent role in determining the size of the shoot system (Nikolaou et al. 2000; Paranychianakis et al. 2004; Sabbatini and Howell 2013), berry formation (Foott et al. 1986; Main et al. 2002), berry quality (Williams and Smith 1991), and yield (Reynolds and Wardle 2001). Given the huge commercial importance of grape and the nearly universal use of rootstocks, a study on the genetics of the root system in grapevine is warranted.

Roots play an important role in the absorption of nutrients and water and therefore are essential for adaptation to widely different soil conditions (Palta and Yang 2014). Root system

architecture refers to the length, thickness, and angle of roots and the branching, density, and spatial arrangement of the root system. (Khan et al. 2016). These traits are governed by the interactions between genetic and environmental factors and determine the regions and volume of the soil explored (Seethepalli et al. 2020). Roots that are narrow-angled tend to grow deep and allow the plant to better absorb water and mineral nutrients such as potassium, calcium, magnesium, and sodium that are available in the deep layers of soil (Borrell et al. 2014). A wide-angled and shallow root system, on the other hand, will allow plants to better absorb nutrients such as nitrogen, carbon, and phosphorus that are found in near-surface layers of soil (Miguel et al. 2015). Recently, substantial scientific attention has been focused on the impact of the three-dimensional structure of roots on plant development and productivity (Giehl et al. 2014; Voss-Fels et al. 2018; Jia et al. 2019).

Finding genes responsible for specific root traits can guide breeders in creating varieties that are well-suited to specific geomorphic and soil conditions. By optimizing RSA features such as specific root length and branching angles, plants increase their capacity for soil exploration (Lynch and Brown 2001; Gahoonia and Nielsen 2004). In various agronomic crops, genomic loci responsible for RSA traits have also been shown to influence crop productivity (Kell 2011; Hufnagel et al. 2014), and the capacity to tolerate drought (Uga et al. 2013). Alahmad et al. (2019) established seven highly significant markers linked to seminal root angle in Durum wheat. Similarly, Manavalan et al. (2010) discovered genes that regulate taproot length and lateral root number in soybeans. Jia et al. (2019) mapped the location of genes controlling root system length, root spread angle, and total seminal root length in spring barley. Alemu et al. (2021) and Maccaferri et al. (2016) found major QTL for seminal root length, root spread angle, number of roots and root and shoot dry weight in Ethiopian tetraploid wheat. Song et al. (2016)

discovered QTL for total root length, lateral root number, primary root length, lateral root density and lateral root length using recombinant inbred maize lines. Several studies have been conducted on the grapevine root system to understand the genetic mechanism for stress tolerance (Corso and Bonghi 2014), root nematode infestation (Smith et al. 2018), and nutrient deficiency (Skinner and Matthews 1990), but none of them has been devoted to directly identifying QTL influencing RSA traits. Understanding the genetic basis of root growth and development will guide breeding efforts to optimize RSA, which will, in turn, improve nutrient acquisition and, adaptability to environmental stress.

Several generations of viticulturists have accumulated a large body of knowledge on the influence of rootstock on the grapevine. Despite the considerable focus on the pivotal role played by rootstocks, the root system has been studied primarily in the context of its impact on the scion (Schenk and Jackson 2002; Smart et al. 2006), and RSA itself has received relatively little attention. Genetic factors govern the emergence of root angles which in turn determines the depth of the root system. It is commonly thought that the rooting pattern of vines is genetically determined and passed down from the parents of the rootstock, but this notion is not supported by strong experimental evidence (Smart et al. 2006). Limited information has been gathered on the genetics of the grapevine root system and almost all of it is anecdotal and relies on observational studies (Smart et al. 2006). Genomic loci and genes that control the development of the grapevine root system and the molecular mechanisms involved have barely been understood. If genomic regions controlling different root features can be identified, breeders can initiate efforts toward tailoring grapevine rootstocks to diverse soil conditions.

In this study, dormant cuttings of F_1 hybrids obtained from the cross between *V. rupestris* X *V. riparia* were rooted and phenotyped for 26 RSA traits. Female parental cuttings also were

rooted and phenotyped alongside the F_1 hybrids. The RSA data were statistically analyzed and variance, heritability, and relationship between root traits and leaf elemental concentration were calculated. Furthermore, QTL analysis was conducted to identify genetic regions that influence RSA traits in the F_1 hybrid progeny.

METHODOLOGY

Plant Materials and Preparation

A panel of 744 dormant F_1 cuttings representing 208 genotypes obtained from the cross between *V. rupestris* Scheele B38 (female parent) and *V. riparia* Michx. HP-1 (male parent) were rooted under controlled conditions and evaluated for various features of RSA. *V. rupestris* is commonly known as rock grape and possesses phylloxera and drought tolerance (Gambetta et al. 2020). It grows in small and isolated populations along stream on the Ozark-Plateau but also occurs sporadically in a narrow crescent-shape region which spreads along Texas, Oklahoma, Arkansas, Kentucky, all the way to the East Coast. *V. riparia* is commonly known as the riverbank grape and it possesses strong phylloxera resistance and tolerance to wet soils (Grzegorczyk and Walker, 1998). Its natural range extends from Canada to Texas, Arkansas, and North Carolina in the north-south direction and from the East Coast to the Rocky Mountains in the east-west direction. The female and male parents were collected in the wild from Texas and South Dakota, respectively, and maintained in the USDA Grape Germplasm Repository in Geneva New York. The cross was made by research geneticist Jason Londo of USDA-ARS. The F_1 hybrid progeny plants were grown at the Darr Agriculture Center at Missouri State University (37º10'20.3" N 93º19'01.1" W). Dormant one-year-old stems (canes) of the thickness of 1.8 cm – 3.1 cm were collected in December 2020 and stored at 4°C for 6 to 8 weeks in moist sawdust to meet chilling requirements. Following storage, the canes were rehydrated by placing them in water for 12 to 24 hours at room temperature. Four average-size canes from each genotype were then cut into two-node sections in such a way that the bottom cut was positioned 2 cm below the lowest bud. The resulting segments were then weighed and inserted 4 cm deep into a 17×13 cm

plastic pot containing moist perlite (**Figure 1**). The potted cuttings were placed in a 6 cm deep tray filled with water. To maintain a constant water table at 12 cm below the surface of the perlite medium, the tray was regularly filled with water. Forty-seven female parental cuttings were also planted side-by-side with F_1 cuttings to compare root traits between maternal and F_1 cuttings. Only 3 *V. riparia* cuttings were retrieved from the Darr Agriculture Center but rooting was unsuccessful in all, therefore I focused this research solely on F_1 population and female parental population.

The experiment was conducted in the Temple Hall Greenhouse at Missouri State University from 14 March to 15 May 2021. The average temperature was 30ºC and with 80% average relative humidity. During the duration of the rooting, no external fertilizer was added to the perlite medium, and the cuttings were irrigated daily.

Root System Photographing and Data Extraction

Rooting was done using the method developed for this thesis. This method relies on perlite medium in a pot, the size which allows unimpeded root growth during the first 5 weeks of adventitious root development, and which facilitates the removal of the plants in a minimally destructive way. At the completion of five weeks, the cuttings with their complete root system were carefully removed from perlite and roots were gently washed under running tap water. The root systems of three cuttings of each genotype that produced the most robust growth were selected for photographing. The washed roots were allowed to drain water in the presence of soft tissue paper. To facilitate consistent light conditions, a backlit cardboard box of the dimension of 40×40×50 cm was prepared with Utopia LSP 22-36 led 61×61 cm LED Edge-Lit panel light on one side and with the opposite side being open for the camera. A hole of 2×2 cm was made on

the top of the box to allow the cutting to protrude in front of the panel light and to place the root system in the field of view of a Basler USB 3.0 monochromatic vision camera, which was connected to a laptop computer. The computer ran the open-source RhizoVision Imager software (Seethepalli et al. 2020) which controlled the camera and performed image acquisition. The camera was placed 40.64 cm away horizontally from the bottom of the cutting where the roots emerged. The root system was rotated into the position in which it created the largest spread across the field of view. The resulting image was a two-dimensional representation of the outline of the entire root system. Only one image of each cutting was taken for analysis. The analysis of the images was done with the help of the open-source software RhizoVision Analyzer (Seethepalli et al. 2020). From each root image, a total of 26 RSA traits, measured in pixels, were extracted using RhizoVision Analyzer (**Table 1**). Upon taking the image of a coin of known width, 370.37 pixels were calculated to be equivalent to a length of 1cm. The values for total root length, depth, maximum width, network area, convex area, lower root area, average diameter, median diameter, maximum diameter, perimeter, volume, and surface area were converted from pixels to length, area, and volume units of the metric system.

Mapping Population, Genotyping, and QTL Mapping

Single nucleotide polymorphisms (SNP) were identified using genotyping-by-sequencing (GBS) reads (Elshire et al. 2011) which aligned to the *V. vinifera* reference genome sequence (RefSeq) at Cornell University, Genomic Center. Using the resulting markers, a high-resolution genetic map of both the male and female parents was created using a heterozygous mapping strategy (Hyma et al. 2015) by Missouri State University graduate student Gaurab Bhattarai (Bhattarai 2019; Bhattarai et al. 2021). Of the traits extracted by RhizoVision Analyzer each

value was Z-scored transformed to generate normally distributed data points. The data obtained from both transformed and untransformed measurement values were used for QTL mapping. A separate mapping table for the female and the male parent, containing both the phenotype and marker data was created. Missing RSA values were noted as N/A in the mapping tables. Each RSA trait was individually tested for QTL using an R script named R/qtl in the female and the male linkage map separately. The R script used for QTL identification in the R/qtl package is shown in **Appendix A**. The Kolmogorov-Smirnov test was conducted to study normality of the data. LOD scores were calculated to determine statistically significant values, where the permutation was carried out 1,000 times. QTL were visualized using LOD graphs, where the significance of the QTL was indicated by the LOD peak crossing the threshold line. Composite interval mapping was chosen over simple interval mapping because it offers an accurate estimate of QTL position, measure of LOD score, and percentage of variance explained. Diagrams that combined linkage maps and LOD graphs were drawn with the help of the graphical software MapChart (Voorrips 2002). Data used to draw diagrams are shown in **Appendices B, C, and D**.

Analysis

Cuttings that developed roots of total length less than 6.7 cm were categorized as outliers and removed from the dataset (**Figure 2**). In total, there were 165 genotypes which had 3 rooted cuttings, and among them 62 were classified as outliers and the remaining 103 were only used for data exploration. Microsoft Excel was used to calculate average values for 26 RSA traits for every genotype using root trait values from 3 rooted cuttings. To compare the RSA traits of the F_1 population and those of female parent (*V. rupestris*), female cuttings were also rooted side-by-side with F_1 vines. Female cuttings were placed at different locations in the greenhouse to expose

the cuttings to microenvironmental variation within the greenhouse. Because the cuttings of the female parent were genetically identical, the phenotypic variance observed in their root system resulted only from microenvironmental differences like temperature and humidity within the greenhouse ($V_{P\ (Female\ parent)} = V_{E\ (Female\ parent)}$). The phenotypic variance (V_P) observed in the F_1 progeny, on the other hand, was the sum of genetic variance (V_G) and environmental variance (V_E). From this it follows that V_G of the F_1 progeny can be calculated using the equation, $V_{G\ (F1\ progeny)} = V_{P\ (F1\ progeny)} - V_{E\ (Female\ parent)}$ (Bayers 2008). Heritability (H^2) was also calculated for all the traits based on the equation $H^2 = V_G\backslash - V_P$ (Davies et al. 2015). The values for environmental variance, phenotypic variance, genetic variance, and heritability were calculated using MS Excel.

To understand the relationship between different RSA traits, Pearson correlation analysis was conducted between all 26 RSA traits, and a heatmap was constructed based on the results using Panda and NumPy libraries available in Python. GraphPad Prism software was also used to perform principal component analysis (PCA) and to study the correlation between individual F_1 root traits and female parental root traits. PCA reduces high dimensional interrelated data to low dimensional data by linear transformation of the original variables to new set of uncorrelated variables, named principal components. In my study, PCA was used to simplify the complexity of the high-dimensional RSA data and find root traits that explain the most variation in the dataset. Root traits that were correlated to each other ($r > 0.70$) were placed in a single group and a trait with the highest phenotypic variation was selected to represent traits included in that group. Root traits which possessed low correlation (< 0.70) with every other RSA trait were represented individually. Seven root traits which represented 26 traits, namely number of root tips, width-to-depth ratio, medium angle frequency, shallow angle frequency, coarse diameter frequency, average hole size and average root orientation were selected for PCA which was

conducted with the help of packages NumPy, pandas, matplotlib.plyplot, seaborn and sklearn, available in Python.

An additional correlation study was conducted to analyze the relationship between root system traits and leaf elemental concentration. Leaf elemental composition data was obtained from a planting of the F_1 progeny in a Columbia, Missouri vineyard. These data were gathered from fully opened leaves collected from the lowest, middle, and top portions of a shoot (labeled as X, Y, and Z leaves) during the month of May, July, and September of 2020. I was able to identify fifty F_1 genotypes for which both elemental concentration and RSA data were available. Correlation analysis was conducted in X, Y and, Z leaves to determine the strength of correlation of RSA traits to various leaf growth stages with the help of packages NumPy, pandas, matplotlib.plyplot and seaborn available in Python. Furthermore, a canonical correspondence analysis (CCA) was also conducted and a CCA biplot was created to study association between the multivariate dataset containing RSA traits and leaf elemental concentration. I expected a unimodal relationship between the RSA traits and leaf elemental concentration, so I choose CCA over other multivariate methods of data analysis. CCA is used to elucidate the relationships between variables present in two different datasets. CCA was conducted on data of seven RSA traits and the concentration of 10 elements. The direction of the vectors signifies the direction of the maximum change in the RSA traits in regard to the ordination axes, while the length of the vector/line represents rate of change in the corresponding direction. In the ordination biplot, the RSA traits are signified by the vector/line and the leaf elemental concentrations are represented by scattered points in the ordination space. The CCA biplot was created using XL STAT software.

RESULTS

Root Trait Heritability and Contrasts Between F1 Progeny and Their Female Parent

Statistical analysis conducted in the RSA dataset that remained after outlier removal revealed high heritability for holes (0.86), number of root tips (0.82), and total root length (0.75). Negative heritability values were found for traits such as average root orientation (-2.46), steep angle frequency (-2.88), medium angle frequency (-2.01), and shallow angle frequency (-1.93) (**Table 2)**. The female parent was found to have lower values for RSA traits that determine the size of the root system when compared to those of the F_1 plants. Unpaired t-test showed that root traits in F_1 population were significantly different to root traits in female population for median number of roots (2.08 ± 0.9 vs. 2.6 ± 1.1; P= 0.0025), maximum number of roots (10.3 ± 3.2 vs. 12.5 ± 4.5; P = 0.0038), number of root tips (91.2 ± 38.8 vs. 163.1 ± 93.3; P = 0.0001), and total root length (26.7 ± 10.1 vs. 36.8 ± 20.5; P = 0.0016) (**Figure 3**).

Correlation Between Various Root Traits and Leaf Elemental Concentrations

Pearson correlation analysis conducted between RSA traits showed that there was a strong negative correlation between fine diameter frequency and coarse diameter frequency which confirmed that this analysis provided meaningful correlation (R) values (**Figure 4**). The strongest correlation was found between total root length and perimeter (0.99), but total root length also strongly correlated with lower root area (0.95). The maximum number of roots was found to correlate with such traits as total root length (0.94) and number of root tips (0.91). Total root length was found to correlate with network area (0.91). Another notable result was that the perimeter of the root system was found to be correlated with holes (0.92) and with lower root

area (0.94). The most notable negative correlation was found between average root diameter and median number of roots (-0.62), maximum number of roots (-0.68), number of root tips (-0.62), total root length (-0.63), depth (-0.62), convex area (-0.64), and perimeter (-0.68).

Overall, no significant correlation was found between RSA traits and the concentration of all elements examined (**Figure 5**). It was found that calcium, manganese, and zinc correlated positively with maximum number of roots (0.4), lower root area (0.4), perimeter (0.4), volume (0.4), surface area (0.5), and holes (0.5). Phosphorus was found to correlate with solidity (0.4), average diameter (0.5), and median diameter (0.5). Nickle showed a negative correlation with median number of roots (-0.5), maximum number of roots (-0.5), number of root tips (-0.4), total root length (-0.4), maximum width (-0.4), network area (-0.4), convex area (-0.5), lower root area (-0.5), perimeter (-0.5), surface area (-0.4), and holes (-0.5). Correlation analysis conducted between X, Y and Z leaves gathered in the month of May, July, September and RSA traits revealed that correlation of sodium, aluminum, phosphorus, nickel, zinc and molybdenum with average diameter, median diameter, average hole size, number of root tips and solidity was highest in the month of July.

Principal Component and Canonical Correspondence Analyses

PCA conducted between grouped traits revealed that PC1 explained 40.03% of the variation which correlated well with medium angle frequency. PC2 explained 23.68% of the variation where it was well correlated with coarse diameter frequency and number of root tips (**Figure 6**).

Potential relationship between root system traits and leaf elemental concentrations were explored using the canonical correspondence analysis. The first two canonical axes explained

81.27% of the root traits- leaf elemental concentration relationship, with the total inertia being 7.44 and the sum of all canonical eigenvalue being 0.005. The ordination of RSA traits and leaf elemental concentration is presented in a CCA biplot (**Figure 7**), where the length of the average root orientation (ARO) and shallow angle frequency (SAF) show stronger correlation with the ordination axis than other RSA traits. Manganese was found to be linked with number of root tips and coarse diameter frequency whereas iron was found to be linked with medium angle frequency. Boron was found to be linked with width-to-depth ratio, meanwhile cadmium and arsenic were found to be linked to average root orientation. In addition, phosphorus showed association with shallow angle frequency and potassium and sulfur demonstrated association with average root orientation and average hole size.

QTL for Root Traits

In total seven QTL peaks were detected by composite interval mapping in the female and the male genome. True marker-linked significant QTL were detected for surface area, maximum width, and total root length on chromosome 2 in the male parent (*V. riparia*). Of these, only surface area and maximum width were found to have normal distribution by the Kolmogorov-Smirnov test. Four further pseudo-marker-linked QTL peaks were detected on both the female and male genome. The details of these latter QTL peaks are not discussed further in the Results section, because they were mapped to pseudo-markers, the application of which entails uncertainties in the highly heterozygous grapevine genome.

A significant QTL detected for maximum width on chromosome 2 in the male parent (*V. riparia*) had a peak LOD score of 4.25 at the genetic position of 23.63 cM (**Figure 8**).

Interestingly, the QTL peak for surface area was also located in the same genetic position of 23.63 cM on chromosome 2 of the male parent with a peak LOD score of 4.33 (**Figure 9**).

Furthermore, another major QTL for total root length was found to reside on chromosome 2 of the male parent (*V. riparia*) at the genetic position of 13.71 cM with a LOD score of 4.362 (**Figure 10**). No significant QTL peak associated with a true marker was found in the female map (*V. rupestris*) for any traits.

DISCUSSION

Identification of QTL controlling root traits is important in viticulture, as breeders can potentially develop grape varieties suited to various geographic and soil conditions. In this study, three significant QTL peak for maximum width, surface area and total root length were identified. A novel method of rooting grape cutting with the use of nutrient-free perlite medium is also presented here. Root traits that increased the size of the root system were found to be positively correlated with each other, whereas average diameter was found to be negatively correlated with traits that increase the size of the root system. Total root length, number of root tips, maximum and median number of roots were found to be significantly different in the female parent compared to those in the F_1 progeny. High heritability was found for holes, number of root tips and total root length whereas negative heritability was recorded for depth, maximum diameter, volume, average root orientation, shallow angle frequency, medium angle frequency and steep angle frequency. Positive correlation was observed between aluminum, calcium, manganese, zinc, and traits that increase the size of the root system whereas negative correlation was detected between nickel and traits that are responsible for the size of the root system. Correlation of ions and RSA traits was found to be highest in leaves at the middle of the shoot collected in July. Furthermore, CCA demonstrated the association between manganese and number of root tips and coarse diameter frequency, whereas medium angle frequency showed association with iron.

In total, seven QTL for root traits were discovered in this study. Among those seven, three QTL namely, maximum width, total root length, and surface area were found linked to true markers. QTL for maximum width and surface area were found at the same genetic locus in

chromosome 2 of the male parent, suggesting that the genetic control for these traits may be related. Four QTL peaks namely, width-to-depth ratio, network area, lower root area, and maximum diameter was found to be linked to pseudo-markers. A pseudo-marker is an artificial marker generated by the R/qtl software at a fixed interval in the genome. Grapes are highly heterozygous; therefore, the imputation of pseudo-markers is unreliable, and for this reason, QTL found in the pseudo markers are only briefly discussed in this thesis. A QTL for the width-to-depth ratio was found in chromosome 11 of the female parent at a genetic position of 43 cM with a peak LOD score of 4.80 (**Figure 11**). A QTL for network area was found on chromosome 8 of the female parent at a genetic position of 3 cM with a peak LOD score of 5.21 (**Figure 12)**. A QTL for the lower root area was detected on chromosome 8 of the female parent at a genetic position of 3cM with a peak LOD score of 4.36 (**Figure 13**), and finally, a QTL peak for maximum diameter was found in chromosome 5 of the male parent at a genetic position of 39 cM with a peak LOD score of 4.60 (**Figure 14**). Recently, new rhAmp-Seq marker-based linkage maps of these parents have been constructed at South Dakota State University. The new set of RSA data gathered in 2022 will be QTL-analyzed using these denser and, therefore more accurate, linkage maps. It is hoped that using these new resources, QTL will be identified without the use of imputed pseudo-markers that will conclusively confirm or refute the presence of QTL at these genomic locations.

Most studies in grapevine RSA have been conducted by excavating vines in the field. These results are poorly reproducible, because features of RSA are influenced by variable soil conditions in the field. The novel method of rooting presented in this thesis is based on a perlite-based medium which provides uniform consistency and offers minimal resistance to root growth. Furthermore, perlite can be entirely washed away from the root system with ease without

damaging the roots. By rooting the cutting for only 5 weeks, the root system remains small enough that is not impeded by the size of the container. Using this method, the young root system can be examined in its natural confirmation and the RSA can be readily phenotyped by photographing it.

Exploratory analysis of the data revealed that certain traits strongly correlated with one another. As expected, traits that determine the size of the root system namely, maximum number of roots, number of root tips, total root length, and perimeter were found to have a strong positive correlation. Average diameter of individual roots, on the other hand, was found to have a negative correlation with total root length (**Figure 4 and 15**) and several other traits that are related to the size of the entire root system, including median number of roots, perimeter, maximum number of roots and number of root tips (**Figure 16**). This may reflect a trade-off between the plant investing its finite resources into either fewer thicker roots or a larger number of thinner roots. The former strategy would lead to a robust but sparse root system, whereas the latter to a fibrous root system composed of thinner roots. Is it possible that the trade-off observed in the F_1 progeny manifests the segregation of alleles encoding different features of the two parents? This raises the intriguing possibility that these distinct RSA characteristics represent different adaptive strategies of the female and the male parent. The former *V. rupestris* is a plant that typically grows along intermittent rivers that can dry out for extended periods of time. In such a habitat, robust, deep-striking roots provide a competitive advantage. The natural habitat of the male parent, *V. riparia*, on the other hand, is the flood plain, the soil of which is often water-logged in the deeper layers. Under such conditions, a shallower, spreading root system is advantageous. Unfortunately, we were unable to collect comparable RSA trait data on the male parent because we did not have access to sufficient propagation material of its genotype.

In place of a direct comparison between the female and the male parental RSA, I made an inference to the features of the male parent by comparing the RSA trait of the female parent to that of the F_1 progeny (**Figure 3**). I found lower values for number of root tips, maximum number of roots and median number of roots in the female parent compared to the F_1 progeny. This suggests that alleles which increase the value for these traits might have been introgressed from the male parent. Currently, new experiments are underway in the Kovacs Lab to root cuttings of 25 distinct genotypes of *V. rupestris* and 25 distinct genotypes of *V. riparia* to examine the possibility that these RSA features reflect the adaptive strategies by these two species.

In grapevine, the negative correlation between average diameter and traits that determine the size of the root system was previously observed by Chapin III (1974). Vines with thin roots better explore the soil for nutrients. Though the negative correlation between root diameter and root length was weak, I observed that with the increase of every 1μm of average root diameter, total root length decreases by 1.216 mm (**Figure 15**). Though the correlation is not significant with an R-square value of only 0.36, this phenomenon deserves further investigation, because traits such as average diameter of root could be useful guide for breeders to develop grape varieties with various RSA features.

Heritability (H^2) was calculated for all traits (**Table 2**). High heritability values were recorded for holes (0.86), number of root tips (0.82), and total root length (0.75). Several traits were observed to have negative heritability. This negative heritability results from the way genetic variance (V_G) of the F_1 progeny was calculated: $V_{G\ (F1\ progeny)} = V_{P\ (F1\ progeny)} - V_{P\ (Female\ parent)}$. When the phenotypic variance of the female parent ($V_{P\ (Female\ parent)}$) was higher than the phenotypic variance of the F_1 progeny ($V_{P\ (F1\ progeny)}$) a negative value of $V_{G\ (F1\ progeny)}$ was

obtained. How could $V_{P\ (Female\ parent)}$ be higher than $V_{P\ (F1\ progeny)}$, when the former results from only environmental variation, and the latter results from the sum of environmental and genetic variation? One possible explanation is that root development in the female parent is inherently hyper-response to environmental influences and its progeny inherited alleles from the male parent that lessen responsiveness to the environment. This points to the possibility that the RSA of the female parent has high plasticity compared to the F_1 population. This would make biological sense because the female parent (*V. rupestris*) grows under extremely non-homogeneous medium in its natural environment. The species *V. rupestris* specialize to grow on gravel bars in and along river and rocky outcrops (hence its English name: rock grape) (Pap et al. 2015). Under such conditions, root development must be nimble and able to adjust its growth to avoid obstacles, and to find water and nutrients that are in limited supply. This requires high potential for plasticity. The species *V. riparia* on the other hand grows in deep moist soil where a more rigidly determined root architecture, that is, lower plasticity, may provide competitive advantage. As pointed out above, comparative experiments are being conducted involving genotypes of *V. rupestris* and *V. riparia* cuttings rooted under the same conditions to test this hypothesis.

Correlation matrix between my greenhouse generated RSA dataset and ionomics data gathered from field-grown vines in Columbia, Missouri revealed that aluminum, calcium, manganese, and zinc were found to have a positive correlation with median number of roots, maximum number of roots, total root length, network area, convex area, lower root area, and perimeter. This positive correlation suggests that the absorption of these nutrients is high in vines with a thin root system. Furthermore, nickel was found to have a negative correlation with traits that increase the fibrousness of the grapevine root system. This may indicate that fibrous root

systems are usually shallow, and nickel is found deep in the soil profile. Additionally, correlation of RSA values with elemental concentration present in X, Y and Z leaves collected in the months of May, July and September was also conducted in this study. This analysis revealed that correlation of RSA with leaf elemental concentrations was higher in the month of July compared to the other months (**Appendix E**). This makes sense, because July is the time when the growth of the vine is at its peak and vines absorb a lot of nutrients from the soil to maintain its growth and development. Furthermore, to study the association between root traits and leaf elemental concentration, CCA was conducted, and the result was graphically demonstrated in a CCA biplot (**Figure 7**). Manganese was found to be associated with number of root tips and coarse diameter frequency. Since spatial variability was observed in studies conducted in manganese composition in soil in various geographic and agronomic conditions (Franzluebbers and Hons 1996; Lu et al. 2004), specific conclusion could not be derived. Iron was found to be associated with medium angle frequency and this makes biological sense as iron is at highest concentration in the sublayer of the soil (Lu et al. 2004) and genotypes with high value for medium angle frequency tend to have deeper root system. Since many of the variables used in this study possessed similar values, the level of resolution remained low. Furthermore, correlation values observed in RSA leaf elemental concentration study were low and definitive conclusions couldn't be derived. Nonetheless this phenomenon deserves further study as RSA features may serve as a good breeding target to tailor rootstock varieties for varying soil conditions. One reason for the low correlation between ion content and RSA was that, at the time of analysis only 50 genotypes with data for both RSA and leaf elemental concentration were available. Replica of all 208 F_1 genotypes analyzed in this work are maintained in experimental vineyards at Geneva, New York, Brookings, South Dakota, and Springfield, Missouri. The relationship between RSA and leaf

elemental concentration will be further explored when leaf elemental concentration from these diverse environmental conditions is overlaid with soil data.

In addition to genetic and soil factors, microorganisms found in soil and the vicinity of root also plays an important role in root system development and growth. The study conducted by Caruso et al. (2021) found increased root length, surface area, and root diameter in fig treated with mycorrhizal culture media. Additionally, Luciani et al. (2019) found increased lateral root length, increased root volume and increased root biomass in grapevines treated with a mycorrhizal fungus. Since this experiment was conducted in perlite medium in greenhouse, effect of mycorrhizal fungus on root growth could not be measured. Future studies need to incorporate the effect of mycorrhiza on root growth to better understand root development and proliferation under natural condition.

REFERENCES

Agüero C, Riaz S, Fort K, Heinitz C, Romero N, Walker MA and Lund K. 2013. Breeding grape rootstocks for resistance to phylloxera and nematodes-it's not always easy. In VI International Phylloxera Symposium 1045:89-97.

Alahmad S, El Hassouni K, Bassi FM, Dinglasan E, Youssef C, Quarry G, Aksoy A, Mazzucotelli E, Juhasz J, Able JA and Christopher J. 2019. A major root architecture QTL responding to water limitation in durum wheat. Front. Plant Sci 10:1–18.

Alemu A, Feyissa T, Maccaferri M, Sciara G, Tuberosa R, Ammar K, Badebo A, Acevedo M, Letta T and Abeyo B. 2021. Genome-wide association analysis unveils novel QTLs for seminal root system architecture traits in Ethiopian durum wheat. BMC Genomics 22:1–16.

Arora NK. 2019. Impact of climate change on agriculture production and its sustainable solutions. J Environ Sustain 2:95-96.

Bayers D. 2008. Components of phenotypic variance. Nature Education 1:161.

Bhattarai G, Fennell A, Londo JP, Coleman C and Kovacs LG. 2021. A novel grape downy mildew resistance locus from *Vitis rupestris*. Am J Enol Vitic 72:12-20.

Bhattarai G. 2019. Mapping a New Disease Resistance Locus in an F1 progeny Derived from Two Grape Wild Relatives. Thesis. Missouri State University, Springfield.

Borrell AK, Mullet JE, George-Jaeggli B, Van Oosterom EJ, Hammer GL, Klein PE and Jordan DR. 2014. Drought adaptation of stay-green sorghum is associated with canopy development, leaf anatomy, root growth, and water uptake. J Exp Bot 65: 6251–6263.

Chapin III FS. 1974. Morphological and physiological mechanisms of temperature compensation in phosphate absorption along a latitudinal gradient. Ecology 55:1180-1198.

Corso M and Bonghi C. 2014. Grapevine rootstock effects on abiotic stress tolerance. Plant Sci Today 1:108-113.

Caruso T, Mafrica R, Bruno M, Vescio R and Sorgona A. 2021. Root architecture traits of two fig cultivars: Treatments with arbuscular mycorrhizal fungi formation. Sci Hortic 283:110083.

Davies SW, Scarpino SV, Pongwarin T, Scott J and Matz MV. 2015. Estimating trait heritability in highly fecund species. G3 5:2639-2645.

Doucleff M, Jin Y, Gao F, Riaz S, Krivanek AF and Walker MA. 2004. A genetic linkage map of grape, utilizing *Vitis rupestris* and *Vitis arizonica*. Theor Appl Genet 109:1178–1187.

Elshire RJ, Glaubitz JC, Sun Q, Poland JA, Kawamoto K, Buckler ES and Mitchelle SE. 2011. A robust, simple genotyping-by-sequencing (GBS) approach for high diversity species. PLoS One 6:e19379.

Franzluebbers AJ and Hons FM. 1996. Soil-profile distribution of primary and secondary plant-avaiable nutients under conventional and no tillage. Soil Till Res 39:229-239.

Foott J, Ough C and Wolpert J. 1986. Rootstock effects on wine grapes. Calif Agric 43:27–29.

Gahoonia TS and Nielsen NE. 2004. Barley genotypes with long root hairs sustain high grain yields in low-P field. Plant Soil 262:55-62.

Gambetta GA, Herrera JC, Dayer S, Feng Q, Hochberg U and Castellarin SD. 2020. The physiology of drought stress in grapevine: towards an integrative definition of drought tolerance. J Exp Bot 71:4658-4676.

Giehl RF, Gruber BD and Von Wirén N. 2014. It's time to make changes: modulation of root system architecture by nutrient signals. J Exp Bot 65:769–778.

Gomez-Zavaglia A, Mejuto JC and Simal-Gandara J. 2020. Mitigation of emerging implications of climate change on food production systems. Int Food Res J 134:109256.

Granett J, Walker MA, Kocsis L and Omer AD. 2001. Biology and management of grape phylloxera. Annu Rev Entomol 46:387.

Grzegorczyk W and Walker MA. 1998. Evaluating resistance to grape phylloxera in *Vitis* species with an in vitro dual culture assay. Am J Enol Vitic 49:17-22.

Hepaksoy S, Ben-Asher J, De Malach Y, David I, Sagih M and Bravdo B. 2006. Grapevine Irrigation with saline water: Effect of rootstock on quality and yield of Cabernet Sauvignon. J Plant Nutr 29:783-795.

Hufnagel B, de Sousa SM, Assis L, Guimaraes CT, Leiser W, Azevedo GC, Negri B, Larson BG, Shaff JE, Pastina MM and Barros BA. 2014. Duplicate and conquer: multiple homologs of PHOSPHORUS-STARVATION TOLERANCE1 enhance phosphorus acquisition and sorghum performance on low-phosphorus soils. Plant Physiol 166:659-677.

Hyma KE, Barba P, Wang M, Londo JP, Acharya CB, Mitchell SE, Sun Q, Reisch B and Cadle-Davidson L. 2015. Heterozygous mapping strategy (HetMappS) for high resolution genotyping-by-sequencing markers: a case study in grapevine. PloS One 10:e0134880.

Jia Z, Liu Y, Gruber BD, Neumann K, Kilian B, Graner A and Von Wiren N. 2019. Genetic dissection of root system architectural traits in spring barley. Front Plant Sci 10:400.

Kell DB. 2011. Breeding crop plants with deep roots: their role in sustainable carbon, nutrient and water sequestration. Ann Bot 108:407–418.

Khan MA, Gemenet DC and Villordon A. 2016. Root system architecture and abiotic stress tolerance: current knowledge in root and tuber crops. Front Plant Sci 7:1584.

Liu X, Zhang Y, Han W, Tang A, Shen J, Cui Z, Vitousek P, Erisman JW, Goulding K, Christie P and Fangmeier A. 2013. Enhanced nitrogen deposition over China. Nature 494:459–462.

Luciani E, Frioni T, Tombesi S, Farinelli D, Gardi T, Ricci A, Sabbatini P and Palliotti A. 2019. Effects of a new arbuscular mycorrhizal fungus (*Glomus iranicum*) on grapevine development. In BIO Web of Conferences Vol. 13, p.04018.

Lu S, Liu X, Li L, Zhang F, Zeng F, Zeng X and Tang C. 2004. Effect of manganese spatial distribution in the soil profile on wheat growth in rice-wheat rotation. Plant Soil 261:39-46.

Lynch JP and Brown KM. 2001. Topsoil foraging–an architectural adaptation of plants to low phosphorus availability. Plant Soil 237:225-237.

Maccaferri M, El-Feki W, Nazemi G, Salvi S, Cane MA, Colalongo MC, Stefanelli S and Tuberosa R. 2016. Prioritizing quantitative trait loci for root system architecture in tetraploid wheat. J Exp Bot 67:1161-1178.

Main G, Morris J and Striegler K. 2002. Rootstock effects on Chardonel productivity, fruit, and wine composition. Am J Enol Vitic 53:37–40.

Manavalan LP, Guttikonda SK, Nguyen VT, Shannon JG and Nguyen HT. 2010. Evaluation of diverse soybean germplasm for root growth and architecture. Plant Soil 330:503-514.

McKenry MV and Anwar SA. 2006. Nematode and grape rootstock interactions including an improved understanding of tolerance. J Nematol 38:312.

McKenry MV, Luvisi D, Anwar SA, Schrader P and Kaku S. 2004. Eight-year nematode study from uniformly designed rootstock trails in fifteen table grape vineyards. Am J Enol Vitic 55:218-227.

Miguel MA, Postma JA and Lynch JP. 2015. Phene synergism between root hair length and basal root growth angle for phosphorus Acquisition. Plant Physiol 167:1430–1439.

Mishra PK. 2017. Socio-ecomomic impacts of climate change in Odisha: issues, challenges and policy options. J Clim Change 3:93-107.

Nikolaou N, Koukourikou M and Karagiannidis N. 2000. Effect of various rootstock on xylem exudates cytokinin content, nutrient uptake and growth pattern of grapevine *Vitis vinifera* L. cv. Thompson seedless. Agronomie 20:363-373.

Ollat N, Bordenave L, Tandonnet JP Boursiquot JM and Marguerit E. 2014. Grapevine rootstocks:origins and perspectives. In I International Symposium on Grapevine Roots 1136 11-22.

Palta JA and Yang J. 2014. Crop root system behaviour and yield. Field Crops Res 165:1–4.

Pap D, Miller AJ, Londo JP and Kovacs LG. 2015. Population structure of *Vitis rupestris,* an important resource for viticulture. Am J Enol Vitic 66:403-410.

Paranychianakis NV, Aggelides S and Angelakis AN. 2004. Influence of rootstock, irrigation level and recycled water on growth and yield of Soultanina grapevines. Agric Water Manag 69:13-27.

Reynolds AG and Wardle DA. 2001. Rootstocks impact vine performance and fruit composition of grapes in British Columbia. Horttechnology 11:419-427.

Sabbatini P and Howell GS. 2013. Rootstock scion interaction and effects on vine vigor, phenology, and cold hardiness of interspecific hybrid grape cultivars (*Vitis* spp.). Int J Fruit Sci 13:466-477.

Schenk HJ and Jackson RB. 2002. Rooting depths, lateral root spreads and below-ground/above-ground allometries of plants in water-limited ecosystems. J Ecol 90:480-494.

Seethepalli A, Guo H, Liu X, Griffiths M, Almtarfi H, Li Z, Liu S, Zare A, Fritschi FB, Blancaflor EB and Ma XF. 2020. RhizoVision Crown: an Integrated hardware and software platform for root crown phenotyping. Plant Phenomics 2020.

Sen Z. 2021. Reservoirs for water supply under climate change impact- a review. Water Resour Manag 35:3827-3843.

Skinner PW and Matthews MA. 1990. A novel interaction of magnesium translocation with the supply of phosphorus to roots of grapevine (*Vitis vinifera* L.). Plant, Cell Environ 13:821-826.

Smart DR, Schwass E, Lakso A and Morano L. 2006. Grapevine rooting patterns: a comprehensive analysis and a review. Am J Enol Vitic 57:89-104.

Smith BP. 2010. Genetic and molecular mapping studies on a population derived from *Vitis vinifera* x *Muscadinia rotundifolia* and genetic diversity of wild *Muscadinia rotundifolia*. Thesis. University of California, Davis.

Smith HM, Smith BP, Morales NB, Moskwa S, Clingeleffer PR and Thomas MR. 2018. SNP markers tightly linked to root knot nematode resistance in grapevine (*Vitis cinerea*) identified by a genotyping-by-sequencing approach followed by Sequenom MassARRAY validation. PLoS One 13:e0193121.

Song W, Wang B, Hauck AL, Dong X, Li J and Lai J. 2016. Genetic dissection of maize seedling root system architecture traits using an ultra-high-density bin-map and a recombinant inbred line population. J Integr Plant Biol 58:266-279.

Uga Y, Sugimoto K, Ogawa S, Rane J, Ishitani M, Hara N, Kitomi Y, Inukai Y, Ono K, Kanno N and Inoue H. 2013. Control of root system architecture by DEEPER ROOTING 1 increases rice yield under drought conditions. Nat Genet 45:1097–1102.

Voorrips R. 2002. MapChart: software for the graphical presentation of linkage maps and QTLs. J Hered 93:77-78.

Voss-Fels KP, Snowdon RJ and Hickey LT. 2018. Designer roots for future crops. Trends Plant Sci 23:957-960.

Walker RR, Blackmore DH, Clingeleffer PR and Correll RL. 2004. Rootstock effects on salt tolerance of irrigated field-grown grapevines (Vitis vinifera L. cv. Sultana) 2. Ion concentrations in leaves and juice. Aust J Grape Wine Res 10:90-99.

Williams LE and Smith RJ. 1991. The effect of rootstock on the partitioning of dry weight, nitrogen and potassium, and root distribution of Cabernet Sauvignon grapevines. Am J Enol Vitic 42:118–122.

Wilmink J, Breuer M and Forneck A. 2022. Effects of grape phylloxera leaf infestation on grapevine growth and yield parameters in commercial vineyards: a pilot study. ONEO One 56: 197-208.

Zhou Y, Massonnet M, Sanjak JS, Cantu D and Gaut BS. 2017. Evolutionary genomics of grape (*Vitis vinifera* ssp. *vinifera*) domestication. Proc Natl Acad Sci U.S.A 11:11715–11720.

Table 1. Twenty-six RSA traits extracted from 2-D images of root system.

Extracted	RhizoVision Analyzer Function
Median and maximum number of roots	A horizontal line scan is performed on each segmented image and the number of roots is recorded to calculate the median and the maximum number of roots.
Number of root tips	Total root tips are counted in a skeletonized image.
Total root length	Total Euclidean distance of medial axis pixels is calculated in a skeletonized image to determine total root length.
Depth, maximum width, and width-to-depth ratio	The maximum depth and maximum width of the root are calculated in the segmented image. The ratio of maximum width to depth of the image is noted as the width-to-depth ratio.
Network area, convex area, and solidity	The total pixel area enclosing roots is calculated and defined as the network area. The minimum size of the convex polygon in which a root can fit is defined as the convex hull and the convex area is calculated by adding the total convex hull area.
Average, median, and maximum diameters	The distance to the nearest non-root pixel is determined to create a circle and the diameter of the root is determined for all root pixels to determine the average, median and maximum diameter for entire RSA.
Perimeter, Volume, and surface area	Total Euclidean distance of contour pixel. Using the diameter calculated above, the sum of all roots containing pixels is noted to calculate volume, and the sum of the perimeter of all root containing excel of the skeletal image is noted to calculate surface area.
Lower root area	The lower root area is the area of the segmented image pixels that are located below the location of the medial axis pixel that has the maximum radius.
Holes and average hole size	The space between the root through which light passes are referred to as holes. Hole size is calculated by measuring the total pixel area
Fine, medium, and coarse diameter frequencies	By taking the diameter reading of each pixel, medial axis is grouped into thin and coarse roots.
Shallow, medium, and steep angle frequencies	Given the skeletal image, for every pixel in the medial axis, the locations of the medial axis pixels in a 40*40-pixel locality are used to determine the orientation of these pixels in the locality. This orientation is noted for every medial axis pixel. These orientation frequencies are grouped less than 30, 60, 90 degrees from the horizontal.

Table 2.Traits measured in the female parent and the F1 progeny. Mean, standard deviation (SD), variance in seed parent, variance in F1, genetic variation (VG) and heritability (H2) calculated for 26 traits obtained listed in Table 1.

Trait	Mean ± SD		Phenotypic Variance (V_P)		V_G	H^2
	♀ Parent	F_1	♀ Parent	F_1		
Median Number of Roots	2.09 ± 0.93	2.68 ± 1.17	0.86	1.37	0.51	0.37
Maximum Number of Roots	10.32 ± 3.26	12.508 ± 4.59	10.65	21.15	10.49	0.49
Number of Root Tips	91.28 ± 38.8	163.12 ± 93.35	1511.42	8715.13	7203.71	0.82
Total root length (cm)	26.73 ± 10.1	36.88 ± 20.51	102.26	420.98	318.71	0.75
Depth (cm)	4.86 ± 0.98	5.09 ± 0.97	0.95	0.94	-0.009	-0.01
Maximum width (cm)	2.14 ± 0.63	2.29 ± 0.63	0.39	0.4	0.006	0.01
Width-to-Depth Ratio	0.46 ± 0.16	0.46 ± 0.11	0.024	0.01	-0.01	-0.87
Network area(cm^2)	1.33 ± 0.41	1.31 ± 0.48	0.17	0.23	0.06	0.25
Convex area (cm^2)	6.41 ± 2.6	7.22 ± 2.82	6.8	7.98	1.17	0.14
Solidity	0.23 ± 0.07	0.207 ± 0.07	0.005	0.004	-0.0006	-0.13
Lower root area (cm^2)	0.89 ± 0.47	0.98 ± 0.45	0.22	0.2	-0.021	-0.1
Average diameter (cm)	0.08 ± 0.02	0.06 ± 0.02	0.0005	0.0007	0.0002	0.31
Median diameter (cm)	0.03 ± 0.009	0.041 ± 0.03	0.00007	0.0009	0.0008	0.91
Maximum diameter(cm)	0.41 ± 0.07	0.39 ± 0.05	0.005	0.003	-0.001	-0.52
Perimeter (cm)	39.79 ± 15.1	52.78 ± 27.23	228.94	741.95	513.006	0.69
Volume (cm^3)	0.33 ± 0.17	0.26 ± 0.12	0.03	0.015	-0.014	-0.95
Surface area (cm)	6.68 ± 2.32	6.75 ± 2.9	5.39	8.45	3.057	0.36
Holes	31.36 ± 28.9	77.43 ± 77.78	839.8	6050.68	5210.88	0.86
Average Hole Size	2266.5±2747	1874.4 ± 1749.8	7548568	3061862	-44867	1.46
Average Root Orientation	54.95 ± 5.88	55.07 ± 3.16	4.68	10.0009	-24.68	-2.46
Shallow Angle Frequency	0.21 ± 0.06	0.21 ± 0.03	0.004	0.001	-0.002	-1.93
Medium Angle Frequency	0.26 ± 0.06	0.26 ± 0.03	0.004	0.001	-0.002	-2.01
Steep Angle Frequency	0.51 ± 0.11	0.52 ± 0.05	0.01	0.003	-0.009	-2.88
Fine Diameter Frequency	0.07 ± 0.03	0.13 ± 0.04	0.001	0.002	0.001	0.51
Medium Diameter Frequency	0.25 ± 0.07	0.27 ± 0.05	0.005	0.003	-0.001	-0.54
Coarse Diameter Frequency	0.66 ± 0.1	0.59 ± 0.1	0.01	0.01	0.0004	0.04

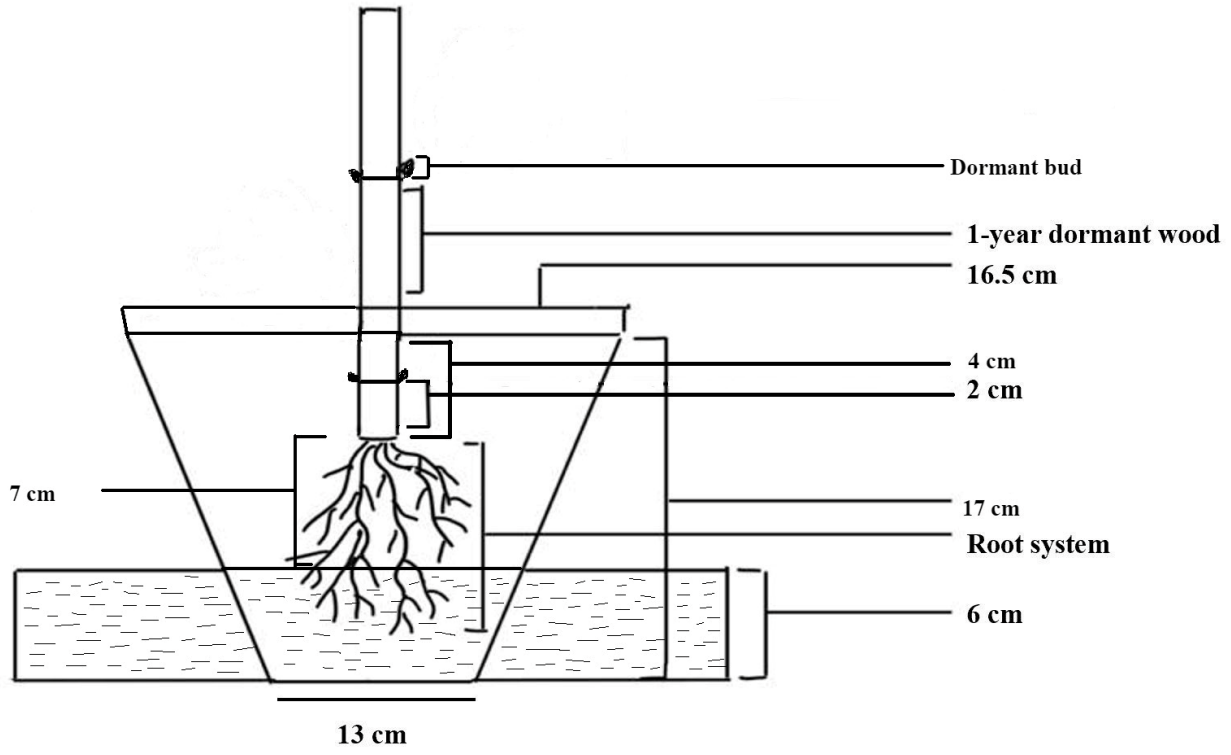

Figure 1. Diagrammatic representation of the experimental setup to root dormant cuttings.

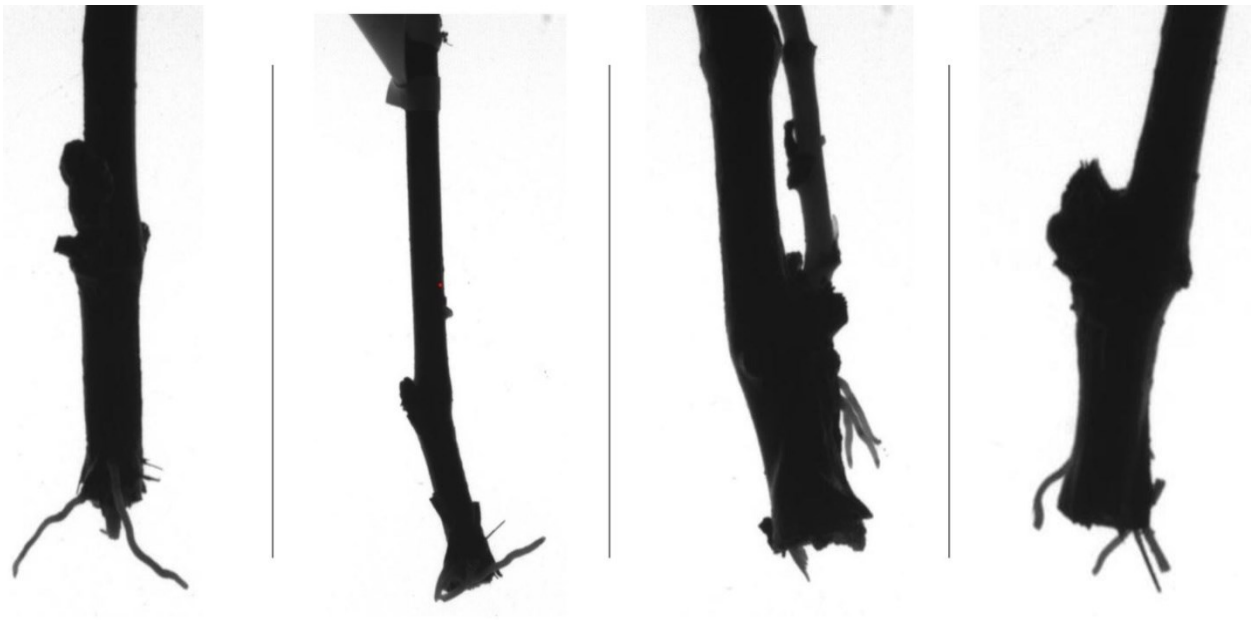

Figure 2. Example of F1 genotypes excluded as outliers from analysis.

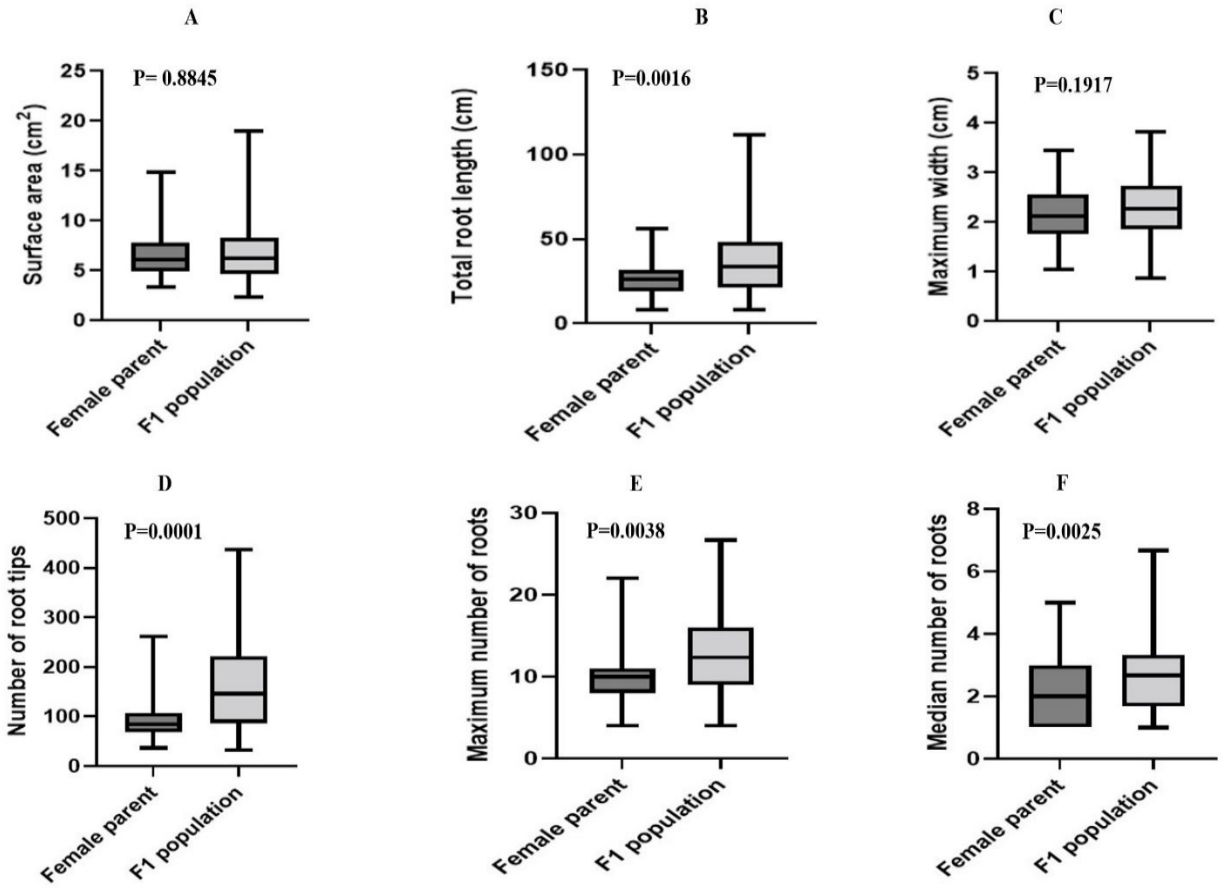

Figure 3. Range of RSA traits of F1 progeny and their female parent. Boxplots of values for maximum width, total root length, and surface area F1 progeny and their female parent.

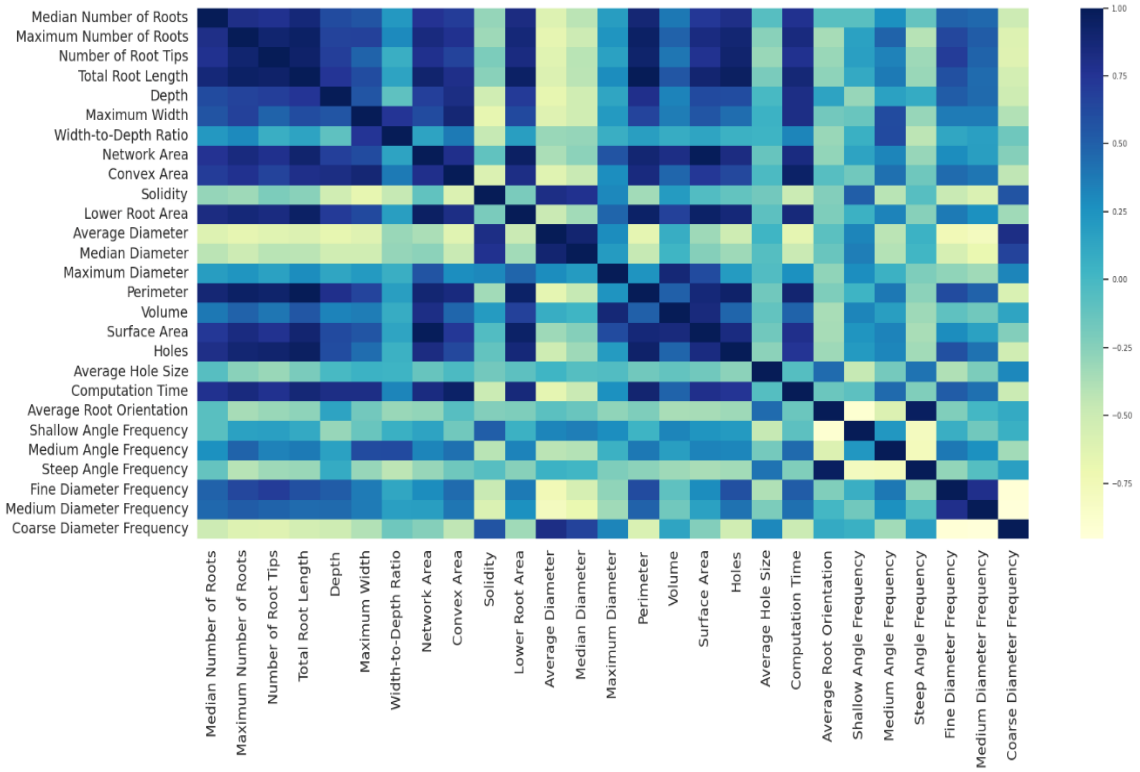

Figure 4. Pearson correlation matrix of RSA traits.

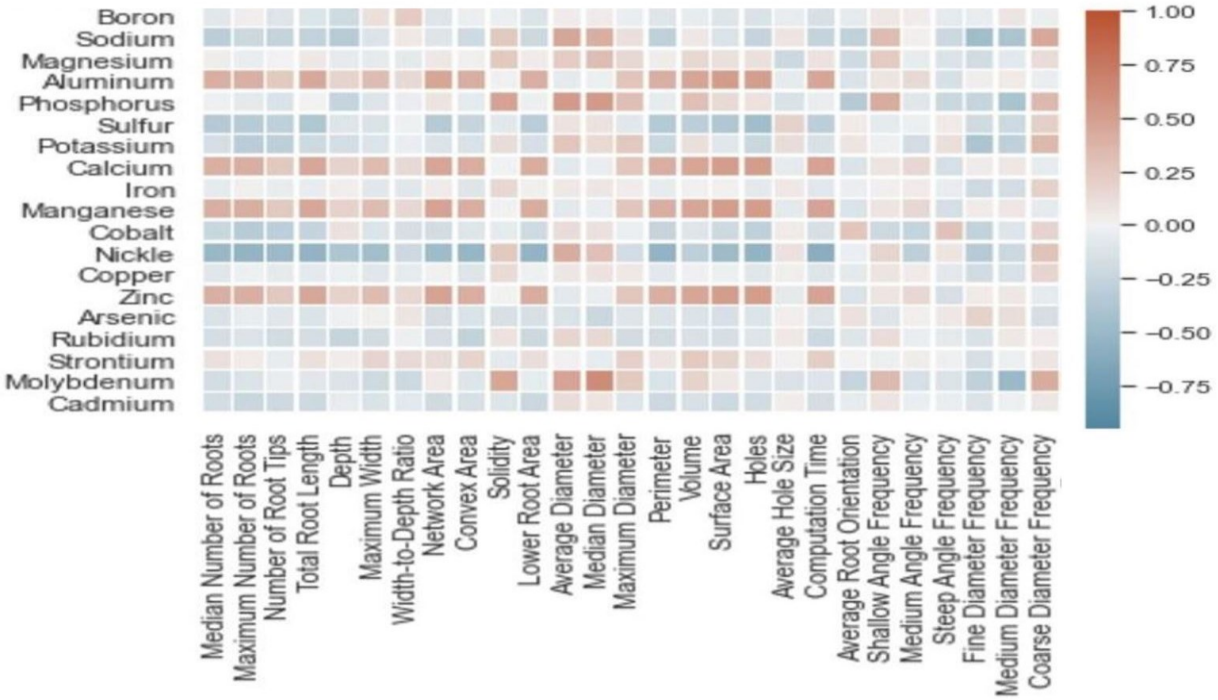

Figure 5. Pearson correlation matrix of RSA traits and leaf elemental concentration

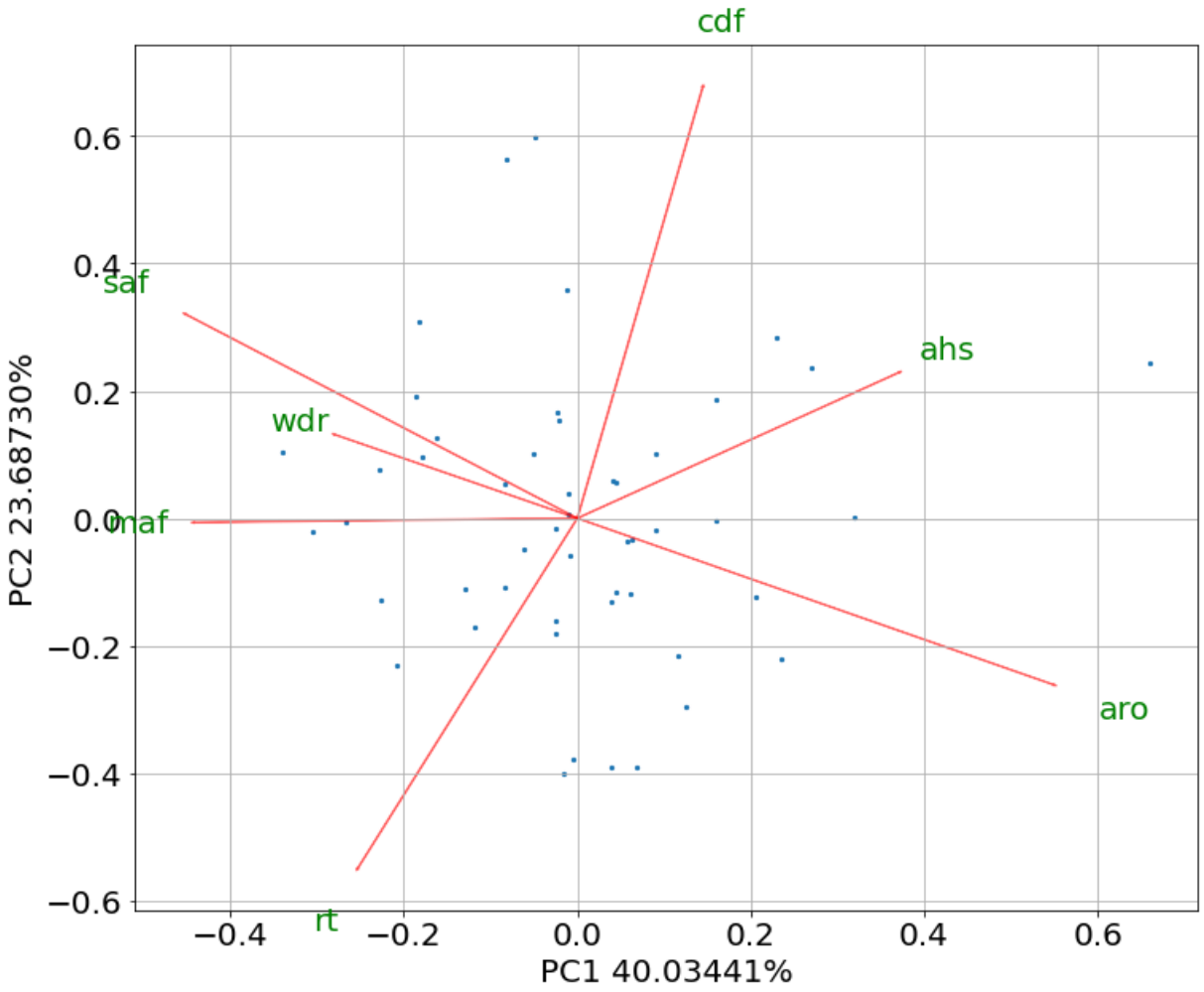

Figure 6. PCA analysis of seven diverse RSA traits. Number of root tips (rt), width-to-depth ratio (wdr), shallow angle frequency (saf), average root orientation (aro), median angle frequency (maf), average hole size (ahs), coarse diameter frequency (caf).

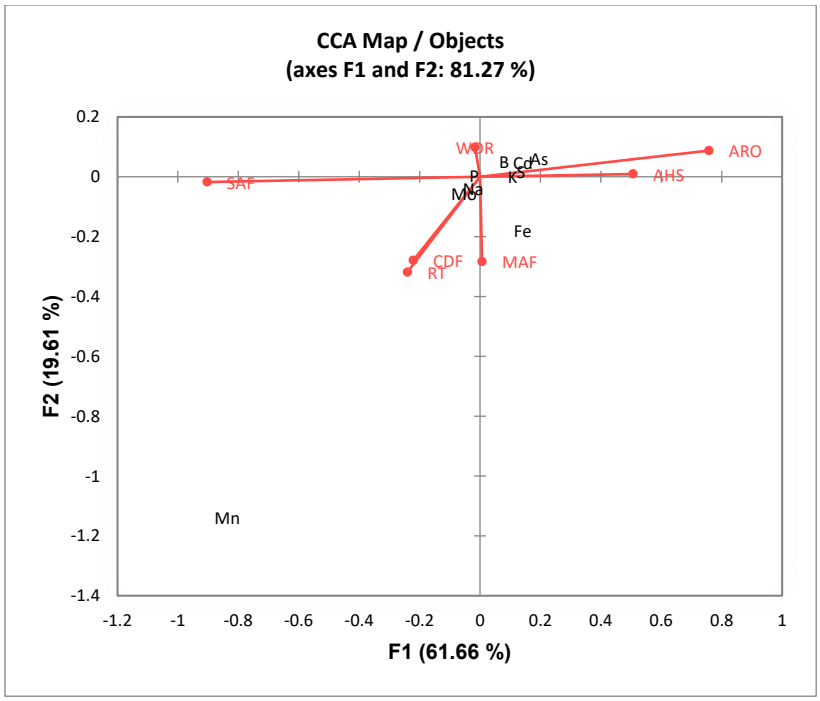

Figure 7. CCA biplot of the relationship between RSA traits and leaf elemental concentration. Number of root tips (rt), width-to-depth ratio (wdr), shallow angle frequency (saf), average root orientation (aro), median angle frequency (maf), average hole size (ahs), coarse diameter frequency (caf), boron (B), sodium (Na), potassium (K), sulphur (S), iron (Fe), manganese (Mn), phosphorus (P), arsenic (A), molybdenum (Mo), cadmium (Cd).

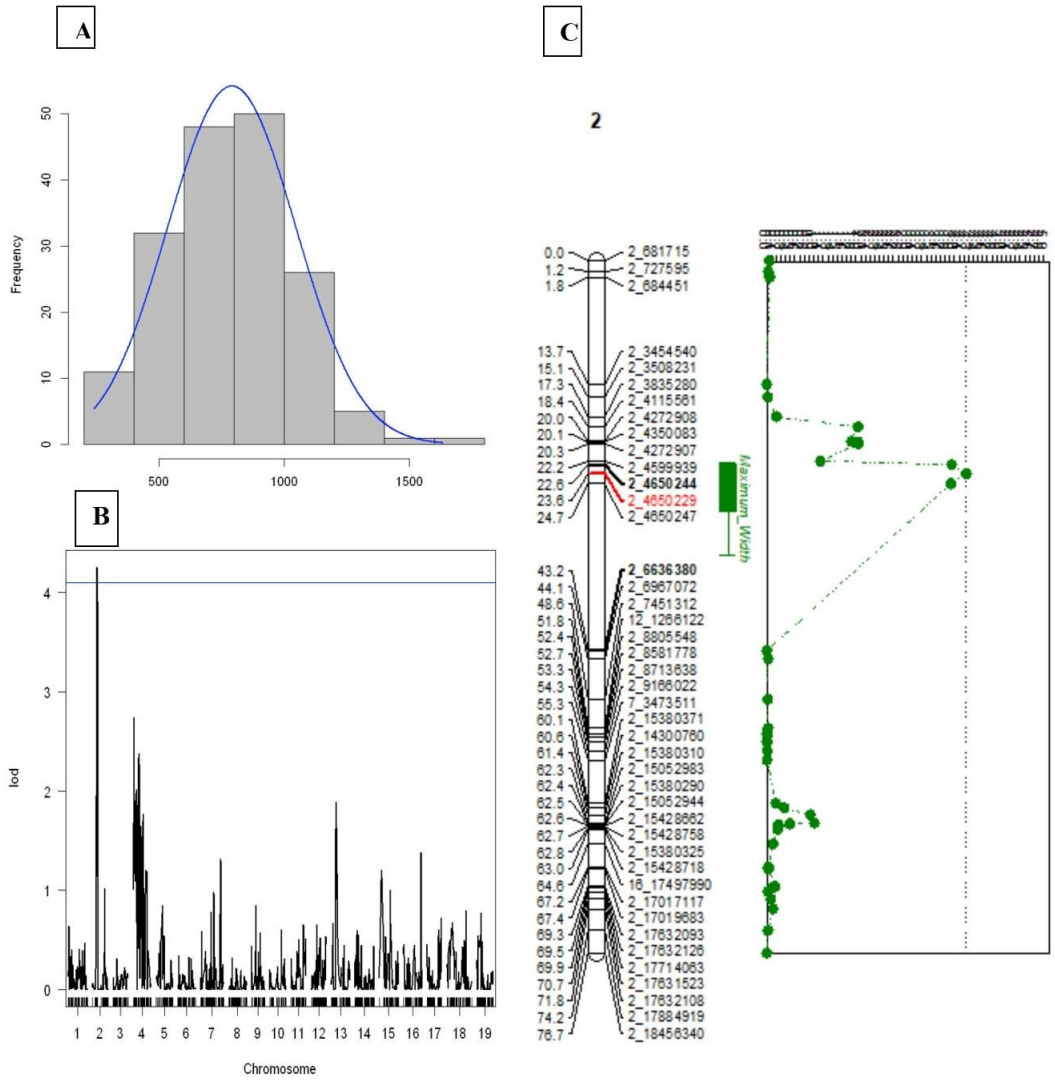

Figure 8. QTL mapping of the maximum width of the root system. (A) Frequency distribution of F_1 progenies for maximum width phenotype. (B) Significant QTL ($p<0.05$) on chr2 of male parent *V. riparia*. (C) LOD graph for maximum width in *V. riparia*. The width of box represents 1-LOD range, and whiskers are 2-LOD range for the QTL peak.

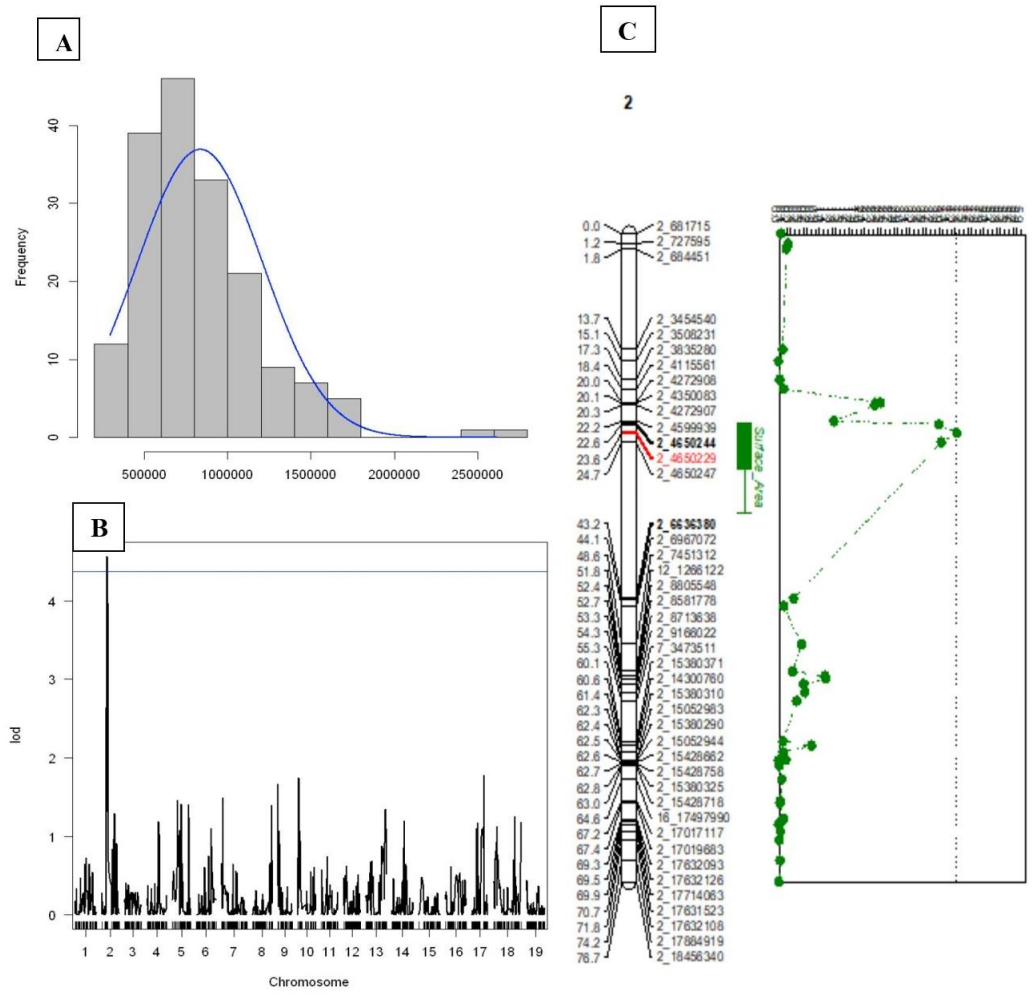

Figure 9. QTL mapping of the surface area of the root system. (A) Frequency distribution of F_1 progenies for surface area phenotype. (B) Significant QTL ($p<0.05$) on chr2 of male parent *V. riparia*. (C) LOD graph for surface area in *V. riparia*. The width of box represents 1-LOD range, and whiskers are 2-LOD range for the QTL peak.

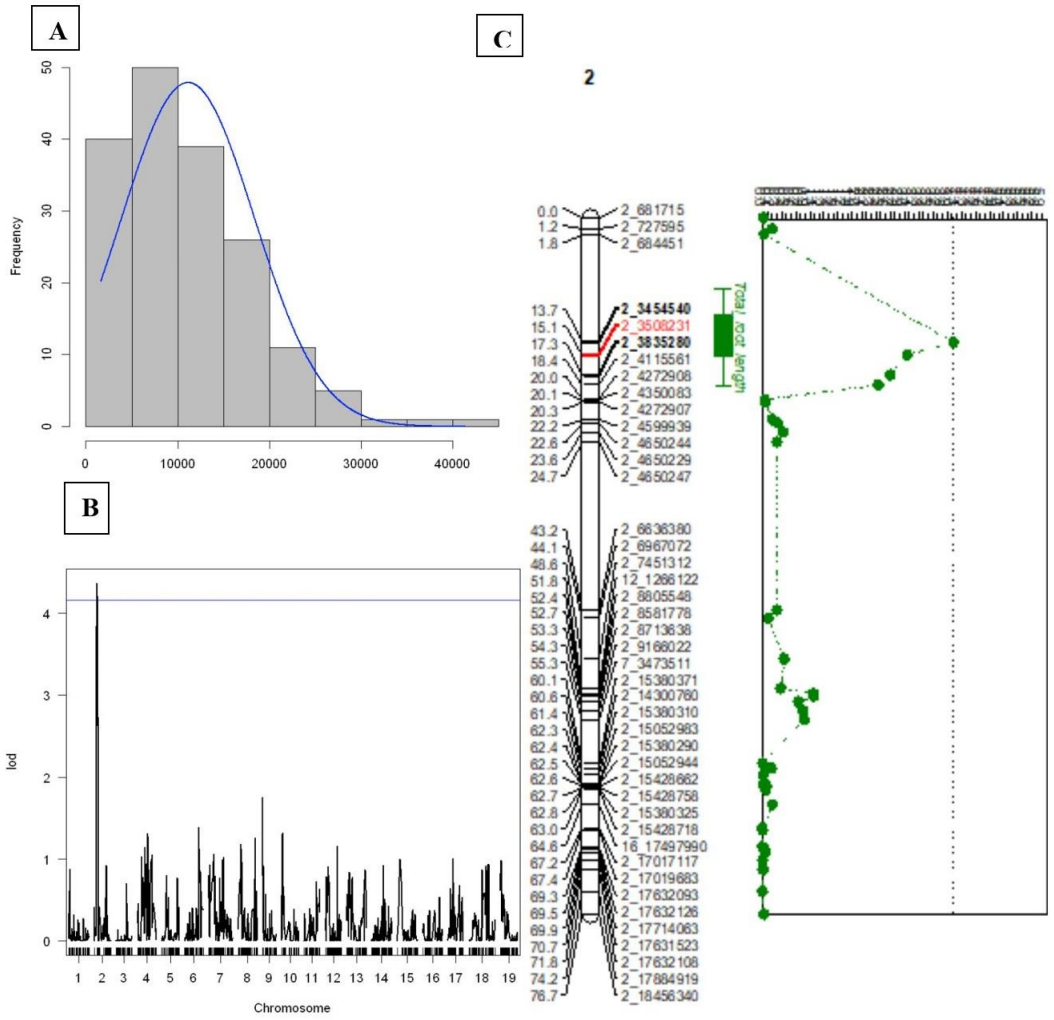

Figure 10. QTL mapping of the total length of the root system. (A) Frequency distribution of F_1 progenies for total root length phenotype. (B) Significant QTL ($p<0.05$) on chr2 of male parent *V. riparia*. (C) LOD graph for total root length in *V. riparia*. The width of box represents 1-LOD range, and whiskers are 2-LOD range for the QTL peak.

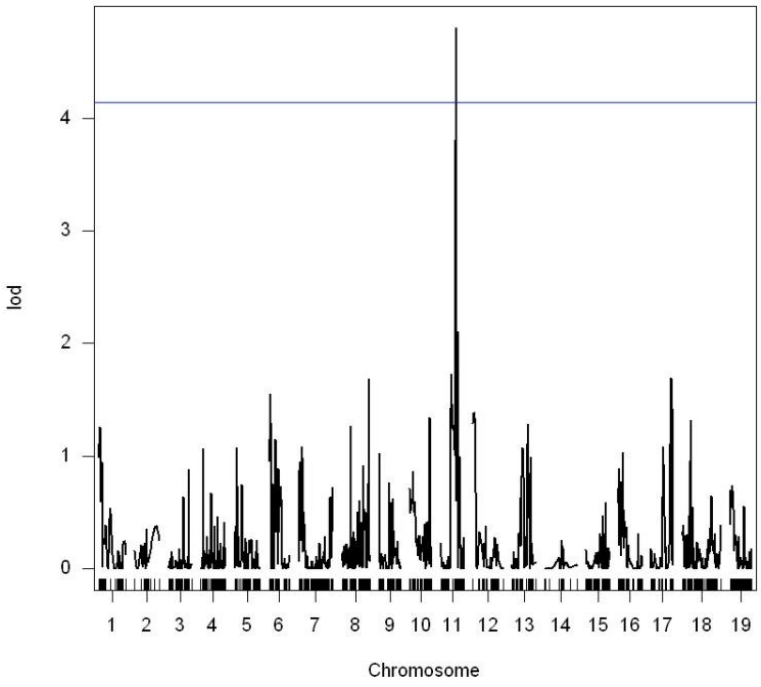

Figure 11. QTL for the width-to-depth ratio. Significant QTL ($p<0.05$) on chr11 of *V.rupestris*. Genome wide LOD thresholds after 1000 permutation was 4.80 at 5% (blue line) level of significance at 43 cM on the genome.

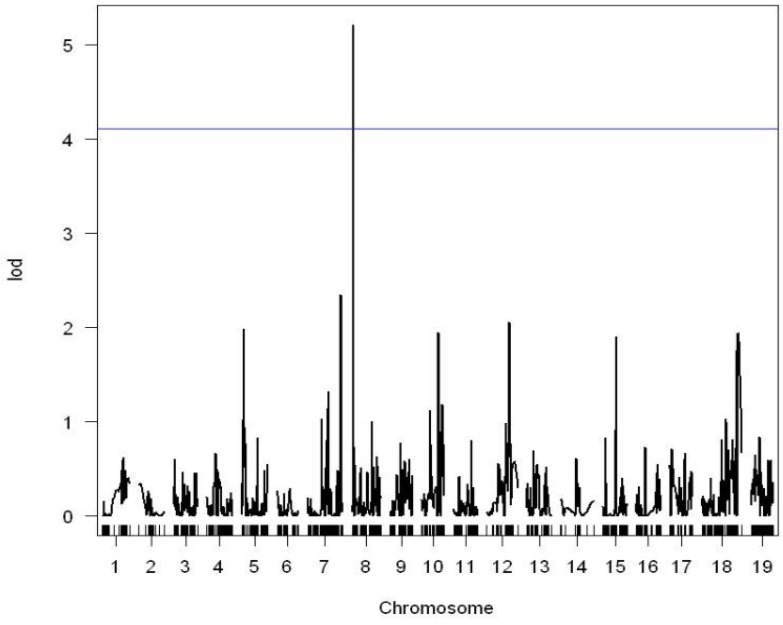

Figure 12. QTL for the network area. Significant QTL ($p<0.05$) on chr8 of V.rupestris. Genome wide LOD thresholds after 1000 permutation was 5.21 at 5% (blue line) level of significance. QTL was located at 3 cM position on the genome.

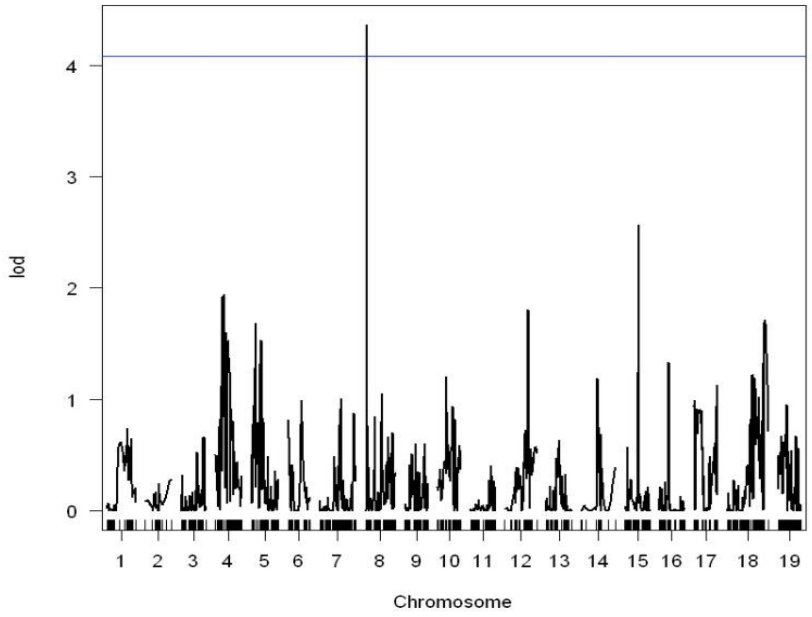

Figure 13. QTL for the lower root area. Significant QTL ($p<0.05$) on chr11 of V.rupestris. Genome wide LOD thresholds after 1000 permutation was 4.36 at 5% (blue line) level of significance. QTL was located at 3 cM position on the genome.

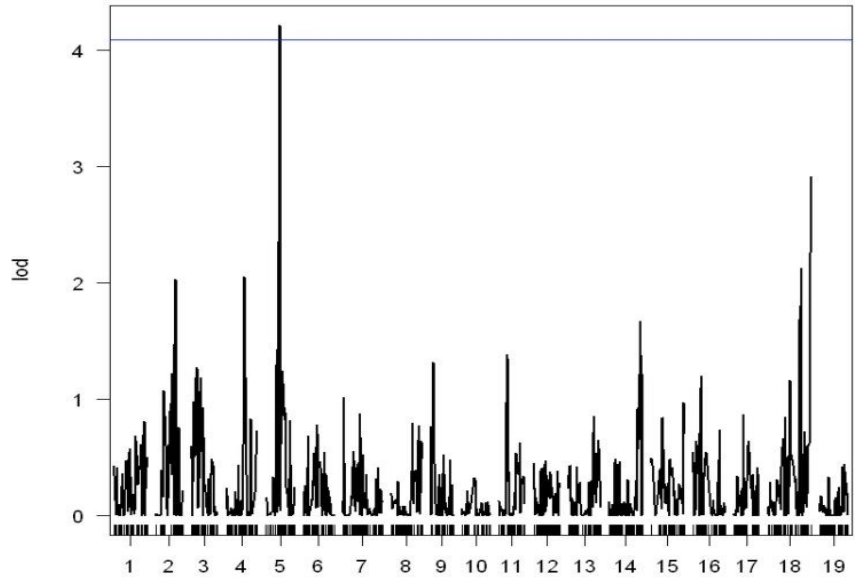

Figure 14. QTL for the maximum diameter. Significant QTL ($p<0.05$) on chr5 of V.riparia. Genome wide LOD thresholds after 1000 permutation was 4.21 at 5% (blue line) level of significance. QTL was located at 39 cM position on the genome.

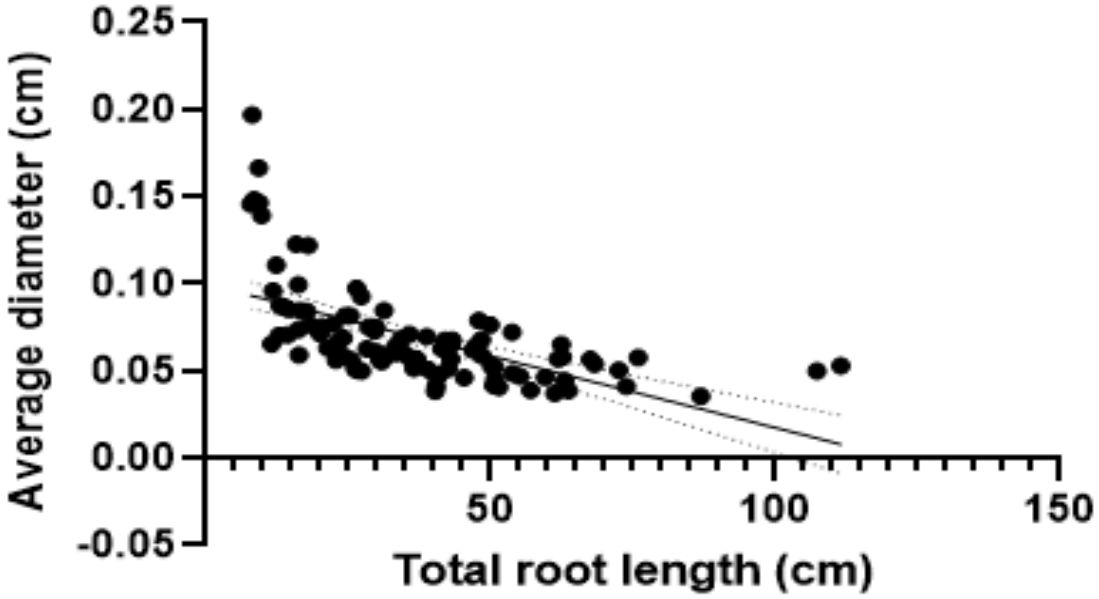

Figure 15. Correlation between average diameter and total root length. The bold line provides the best estimate of average diameter while dotted line indicates 95% confidence intervals.

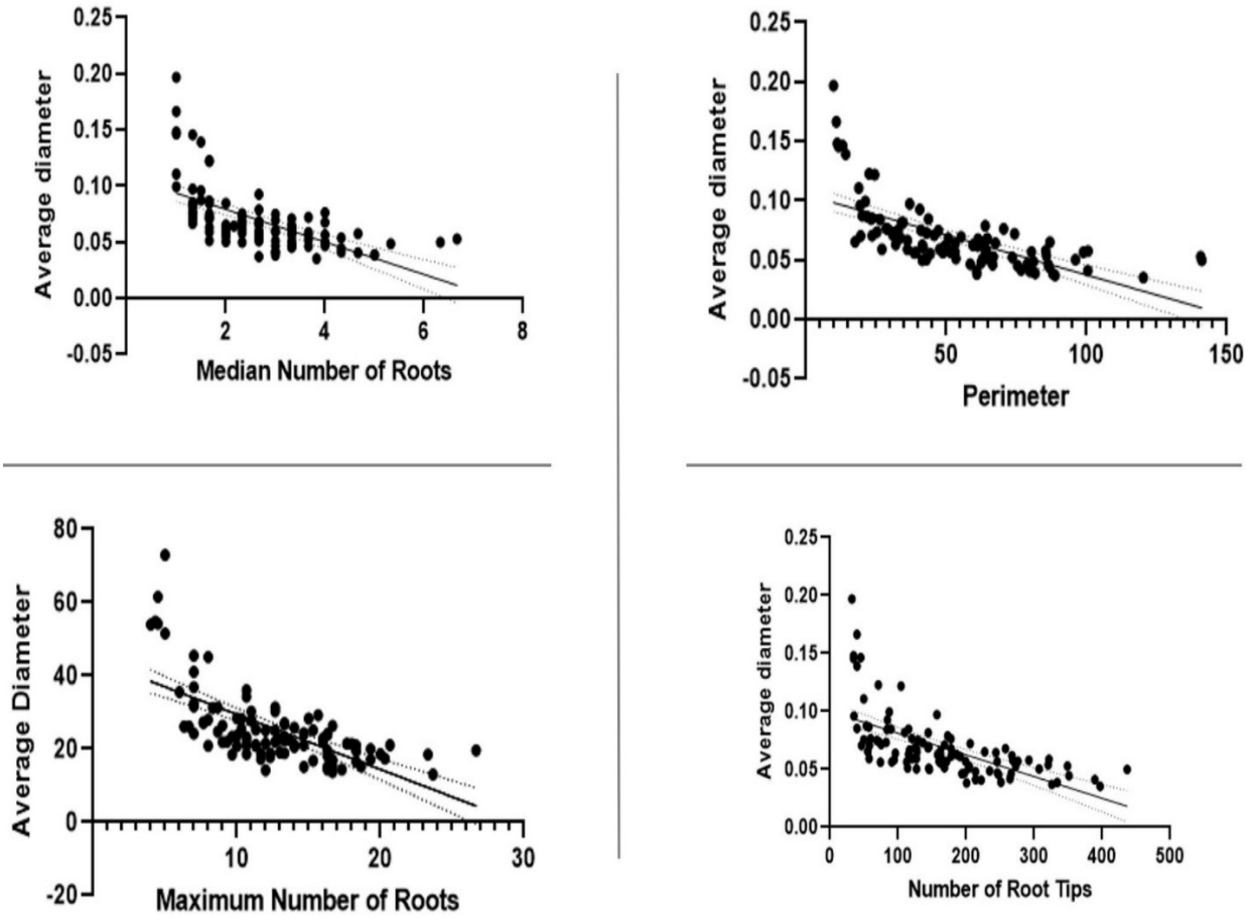

Figure 16. Correlation between average diameter and root size determining traits. The bold line provides the best estimate of average diameter while dotted line indicates 95% confidence intervals.

APPENDICES

Appendix A. Script used in R/qtl for QTL peak detection

```
install.packages('qtl') #Main package, for analysis
install.packages('qtlcharts') #accessory, for displaying graphs
install.packages('LinkageMapView') #accessory, for displaying linkage maps
install.packages('rcompanion')# for plotNormalHistogram|

library(qtl) #load packages
library(qtlcharts)
library(LinkageMapView)
library(rcompanion)

#Collecting enviroment variables
print("Make sure to input names AS THEY APPEAR on the csv!!") #Just a user warning
fileName <- readline("Enter file name (Either FemaleMap.csv or MaleMap.csv): ") #Mappng
table file
genotypeName <- c(readline("First Genotype (homozygous) (For example ll): "),
readline("Second Genotype (heterozygous) (for example lm): ")) #For example "nn", "np"
alleleName <- c(substr(genotypeName[2],1,1) ,substr(genotypeName[2],2,2))
naNames <- c("NA","--") #For example "NA", "--"
colNum <- as.numeric(readline("Column Number: ")) #Column for pheno of interest

#Map generation
Map <- read.cross(format = 'csv',file = fileName ,genotypes = genotypeName,
alleles = alleleName,na.strings = naNames) #generate linkage map
Map <- jittermap(Map) #make sure no markers are in the same location
Map <- calc.genoprob(Map,step = 1,map.function = "kosambi") #associate markers with full
genotypes
plot.map(Map) #draw linkage map

plotNormalHistogram(Map$pheno[,colNum]) #normal histogram of pheno of interest

#Compute statistically significant values
TraitCIM1000 <- cim(Map,pheno.col = colNum,method = "hk",
map.function = "kosambi",n.perm = 1000) # Function will take a moment to run, determines
LOD value
plot(TraitCIM1000,col = 'green') #show distribution of lod scores
summary(TraitCIM1000,alpha=c(.05,.01))

#Deterime LOD Values
LOD5 <- summary(TraitCIM1000,alpha=c(.05))
```

```
TraitCIM<-cim(Map,pheno.col = colNum,method = "hk",
map.function = "kosambi") #Generate LOD Values
plot(TraitCIM) #show LOD graph
abline(h = LOD5,col = "blue") #overlay statistically significant line
print("If nothing shows up, the values
are below the LOD5 score") #warning for no peaks
summary(TraitCIM)
write.csv(TraitCIM,"lower root area_FemaleTable.csv")

#Chromosomal Analysis
chr <- as.numeric(readline("Chromosome? ")) #collect chromosome to look at
plot(TraitCIM, chr = chr,xlab = c("chr",chr)) #Plot chr LOD scores
abline(h = LOD5, col = "blue") #Statistically Significant

bayesint(TraitCIM, chr = chr, prob=0.95, expandtomarkers=TRUE) #calculate bayesian interval
lodint(TraitCIM, chr = chr,expandtomarkers = TRUE ) #calculate LOD Support interval

p <- as.numeric(readline("Position for analysis: "))
qtl <- makeqtl(Map, chr = chr, pos = p, what="prob") #pulls genotype probabilities
fitqtl <- fitqtl(Map, pheno.col=colNum, qtl = qtl, covar=NULL,
 method= "hk",model="normal",
 dropone=TRUE, get.ests=TRUE,run.checks=TRUE,
 tol=1e-4, maxit=1000, forceXcovar=FALSE) #sees how well our data fits a given formula
# If you see "error: object of type 'closure' is not subsettable", remove "formula," from the fitqtl
argument list.
summary(fitqtl) #Print results of the analysis
```

Appendix B. Data used to create diagram for maximum width QTL in MapChart

Map	Chr	LOD	Locus
0	2	0.049430316	2_681715
1.211001	2	0.02292941	2_727595
1.835002	2	0.063213965	2_684451
13.710003	2	9.79E-05	2_3454540
15.118004	2	0.017905905	2_3508231
17.297005	2	0.20558011	2_3835280
18.351006	2	1.943299364	2_4115561
20.037007	2	1.802738012	2_4272908
20.051008	2	1.94985369	2_4350083
20.323009	2	1.943598883	2_4272907
22.23201	2	1.145632006	2_4599939
22.623011	2	3.944391513	2_4650244
23.635012	2	4.252665773	2_4650229
24.683013	2	3.921790713	2_4650247
43.199014	2	0.000582665	2_6636380

44.144015	2	0.026804327	2_6967072
48.627016	2	0.014809562	2_7451312
51.763017	2	0.024749724	12_1266122
52.380018	2	0.002508728	2_8805548
52.717019	2	0.003657088	2_8581778
53.28002	2	0.004286252	2_8713638
54.287021	2	0.00910431	2_9166022
55.293022	2	7.80E-06	7_3473511
60.100023	2	0.195123634	2_15380371
60.648024	2	0.369505789	2_14300760
61.423025	2	0.922842911	2_15380310
62.264026	2	1.018507398	2_15052983
62.406027	2	0.49001451	2_15380290
62.502028	2	0.241468755	2_15052944
62.640029	2	0.24143767	2_15428662
62.66703	2	0.241437727	2_15428758
62.817031	2	0.241436833	2_15380325
63.004032	2	0.229389604	2_15428718
64.641033	2	0.133195423	16_17497990
67.249034	2	0.035538598	2_17017117
67.437035	2	0.030352197	2_17019683
69.255036	2	0.17270947	2_17632093
69.545037	2	0.111683065	2_17632126
69.930038	2	0.025577224	2_17714063
70.746039	2	0.085597993	2_17631523
71.78004	2	0.133093642	2_17632108
74.190041	2	0.025870613	2_17884919
76.731042	2	0.000125101	2_18456340

Appendix C. Data used to create diagram for surface area QTL in MapChart

Map	Chr	LOD	Locus
0	2	0.060024281	2_681715
1.211001	2	0.232993158	2_727595
1.835002	2	0.191240292	2_684451
13.710003	2	0.103645241	2_3454540
15.118004	2	6.53E-05	2_3508231
17.297005	2	0.031696885	2_3835280
18.351006	2	0.125117823	2_4115561
20.037007	2	2.480026183	2_4272908
20.051008	2	2.351806706	2_4350083
20.323009	2	2.349629121	2_4272907
22.23201	2	1.349341939	2_4599939
22.623011	2	3.899957021	2_4650244
23.635012	2	4.334125808	2_4650229

24.683013	2	3.959909192	2_4650247
43.199014	2	0.363875345	2_6636380
44.144015	2	0.126529341	2_6967072
48.627016	2	0.557823489	2_7451312
51.763017	2	0.347042648	12_1266122
52.380018	2	1.133929752	2_8805548
52.717019	2	1.14222338	2_8581778
53.28002	2	0.60760569	2_8713638
54.287021	2	0.6401301	2_9166022
55.293022	2	0.442734049	7_3473511
60.100023	2	0.108359557	2_15380371
60.648024	2	0.808517155	2_14300760
61.423025	2	0.109897633	2_15380310
62.264026	2	0.179164489	2_15052983
62.406027	2	0.00434575	2_15380290
62.502028	2	0.014237622	2_15052944
62.640029	2	0.014243549	2_15428662
62.66703	2	0.01424352	2_15428758
62.817031	2	0.014243584	2_15380325
63.004032	2	0.014988394	2_15428718
64.641033	2	0.078911123	16_17497990
67.249034	2	0.045926234	2_17017117
67.437035	2	0.036165751	2_17019683
69.255036	2	0.123123304	2_17632093
69.545037	2	0.064349076	2_17632126
69.930038	2	0.001770611	2_17714063
70.746039	2	0.040329835	2_17631523
71.78004	2	0.014972804	2_17632108
74.190041	2	0.041134752	2_17884919
76.731042	2	0.006074751	2_18456340

Appendix D. Data used to create diagram for total root length QTL in MapChart

Map	Chr	LOD	Locus
0	2	0.020886444	2_681715
1.211001	2	0.202790254	2_727595
1.835002	2	0.036386357	2_684451
13.710003	2	4.03964924	2_3454540
15.118004	2	3.062592679	2_3508231
17.297005	2	2.702456139	2_3835280
18.351006	2	2.450145938	2_4115561
20.037007	2	0.050436812	2_4272908
20.051008	2	0.051773726	2_4350083
20.323009	2	0.05653665	2_4272907
22.23201	2	0.205814308	2_4599939

22.623011	2	0.313145508	2_4650244
23.635012	2	0.439405299	2_4650229
24.683013	2	0.303041675	2_4650247
43.199014	2	0.308840926	2_6636380
44.144015	2	0.128711785	2_6967072
48.627016	2	0.461574728	2_7451312
51.763017	2	0.387045171	12_1266122
52.380018	2	1.077771539	2_8805548
52.717019	2	1.08742078	2_8581778
53.28002	2	0.754788055	2_8713638
54.287021	2	0.859011404	2_9166022
55.293022	2	0.882762916	7_3473511
60.100023	2	0.003365589	2_15380371
60.648024	2	0.192566238	2_14300760
61.423025	2	0.00893183	2_15380310
62.264026	2	0.034354538	2_15052983
62.406027	2	0.017215619	2_15380290
62.502028	2	0.078367768	2_15052944
62.640029	2	0.078378291	2_15428662
62.66703	2	0.078378193	2_15428758
62.817031	2	0.078377678	2_15380325
63.004032	2	0.07190137	2_15428718
64.641033	2	0.214445994	16_17497990
67.249034	2	0.000412677	2_17017117
67.437035	2	0.004622044	2_17019683
69.255036	2	0.000222045	2_17632093
69.545037	2	0.026964604	2_17632126
69.930038	2	0.068072222	2_17714063
70.746039	2	0.007150205	2_17631523
71.78004	2	0.013648553	2_17632108
74.190041	2	0.000827447	2_17884919
76.731042	2	0.027234003	2_18456340

Appendix E. Correlation values between root traits and leaf elemental concentration through various growth stages

	May			July			September		
Correlation	X	Y	Z	X	Y	Z	X	Y	Z
Sodium-Average diameter	0.16	0.04	0.04	-0.15	0.46	0.11	0.09	-0.15	-0.25
Aluminum-Average hole size	0.64	0.43	0.59	-0.11	0.07	0.5	0.06	0.09	-0.18
Phosphorus-Average diameter	0.03	-0.2	0.18	0.1	0.67	0.62	-0.09	0.09	0.02
Phosphorus-Median diameter	0.03	-0.2	0.01	0.1	0.65	0.73	0.05	0.02	0.01
Nickel-Number of root tips	-0.05	0.06	0.28	0.3	-0.39	-0.31	-0.12	-0.13	-0.21
Nickel-Average diameter	0.02	-0.03	-0.18	-0.08	0.46	0.32	0.07	-0.09	0.06
Zinc-Median diameter	0.32	0.61	0.08	0.03	0.1	0.3	-0.23	0.01	-0.18
Molybdenum-solidity	0.06	-0.02	0.06	0.3	0.47	0.49	-0.09	0.05	-0.21
Molybdenum-Average diameter	0.03	0.16	0.2	0.3	0.47	0.57	-0.15	0.04	0.24
Molybdenum-Median diameter	0.04	0.19	0.2	0.3	0.62	0.73	-0.14	-0.05	0.37